

Mesothelium of the Murine Allantois Exhibits Distinct Regional Properties

Jacob M. Daane,¹ Allen C. Enders,² and Karen M. Downs^{1*}

¹*Department of Anatomy, University of Wisconsin-Madison, School of Medicine and Public Health, Madison, Wisconsin 53706*

²*Department of Cell Biology and Human Anatomy, University of California-Davis, Davis, California 95616*

ABSTRACT The rodent allantois is thought to be unique amongst mammals in not having an endodermal component. Here, we have investigated the mesothelium, or outer surface, of murine umbilical precursor tissue, the allantois (~7.25–8.5 days postcoitum, dpc) to discover whether it exhibits the properties of an epithelium. A combination of morphology, challenge with biotinylated dextran amines (BDAs), and immunohistochemistry revealed that the mesothelium of the mouse allantois exhibits distinct regional properties. By headfold stages (~7.75–8.0 dpc), distal mesothelium was generally squamous in shape, and highly permeable to BDA challenge, whereas ventral proximal mesothelium, referred to as “ventral cuboidal mesothelium” (VCM) for the characteristic cuboidal shape of its cells, was relatively impermeable. Although “dorsal cuboidal mesothelium” (DCM) resembled the VCM in cell shape, its permeability to BDA was intermediate between the other two regions. Results of immunostaining for Zonula Occludens-1 (ZO-1) and Epithelial-cadherin (E-cadherin), together with transmission electron microscopy (TEM), suggested that impermeability in the VCM may be due to greater cellular contact area between cells and close packing rather than to maturity of tight junctions, the latter of which, by comparison with the visceral yolk sac, appeared to be rare or absent from the allantoic surface. Both VCM and DCM exhibited an ultrastructure more favorable for protein synthesis than did the distal squamous mesothelium; however, at most stages, VCM exhibited robust afadin (AF-6), whereas the DCM uniquely contained alpha-4-integrin. These observations demonstrate that the allantoic mesothelium is not a conventional epithelium but possesses regional ultrastructural, functional and molecular differences that may play important roles in the correct deployment of the umbilical cord and its associated vascular, hematopoietic, and other cell types. *J. Morphol.* 272:536–556, 2011. © 2011 Wiley-Liss, Inc.

KEY WORDS: adherens junctions; afadin; E-cadherin; epithelium; omphalomesenteric artery, patterning; permeability; umbilical cord; vasculature; visceral endoderm; yolk sac; zonula occludens

INTRODUCTION

Despite its importance in survival of the fetus, little is known about the genesis of the umbilical cord in any amniote. Although details may vary amongst species, the mouse allantois is a model, at least to a

first approximation, for the study of umbilical development. Like that of other amniotes, the allantois issues from the caudal extremity of the embryo, elongates through the exocoelom, and establishes an umbilical vasculature that amalgamates with those of the fetus and nearby yolk sac. In all eutherian species, including rodents, monkeys and humans, the allantois vascularizes the chorion to form an intimate interface for exchange of nutrients, wastes, and gases with the mother.

For many years, the two recognized components of the murine allantois have been the inner core cells, and the outer surface, called “mesothelium” (Downs, 1998). Results of recent experiments have provided evidence that the core of the murine allantois is more complex than was previously suspected. The posterior end of the primitive streak, or embryonic antero-posterior (A-P) axis, reaches into the extraembryonic region (Downs, 2009) where it collaborates with visceral endoderm to establish the allantoic bud (Downs et al., 2009), and a putative stem cell reservoir, the allantoic core domain (ACD) situated within the base of the allantois. The ACD is required for allantoic elongation through the exocoelomic cavity (Downs et al., 2009).

Allantoic mesothelium lies adjacent to the neighboring amnion and yolk sac during the period when the allantois elongates through the exocoelom; ultimately, distal mesothelium of the allantois makes contact with the chorion mesoderm and unites with it (Downs, 2002). However, the

Contract grant sponsor: March of Dimes; Contract grant numbers: #1-FY06-355 and #1-FY09-511; Contract grant sponsor: National Institutes of Child Health and Development; Contract grant number: RO1 HD042706; Contract grant sponsor: University of Wisconsin-Madison.

*Correspondence to: Karen M. Downs, Department of Anatomy, University of Wisconsin-Madison, School of Medicine and Public Health, Madison, WI 53706. E-mail: kdowns@wisc.edu

Received 15 July 2010; Revised 18 October 2010; Accepted 25 October 2010

Published online 31 January 2011 in Wiley Online Library (wileyonlinelibrary.com)
DOI: 10.1002/jmor.10928

properties of mesothelium are obscure. Although the term "mesothelium" (Snell and Stevens, 1966) likely refers to the idea that this tissue is an epithelium derived from mesoderm, the epithelial nature of mesothelium has not been explored in any detail.

Reciprocal allantois/chorion grafting experiments demonstrated that it is the maturity of the allantoic mesothelium that mediates chorio-allantoic union (Downs and Gardner, 1995) in part through the gradual acquisition of vascular cell adhesion molecule-1 (VCAM-1; Downs, 2002) which, with its counter-receptor, alpha-4-integrin, found constitutively on the chorion (Downs, 2002), is essential for formation of the chorio-allantoic labyrinth (Yang et al., 1993; Gurtner et al., 1995; Kwee et al., 1995). In addition, recent studies have suggested that the mesothelium may have hematopoietic potential, as Runx1-positive cells, indicative of definitive hematopoiesis, were found on the allantoic surface (Zeigler et al., 2006). Finally, although other gene products have been systematically documented on the surface of the allantois, including Bone Morphogenetic Protein-4 (BMP-4; Lawson et al., 1999; Downs et al., 2004), Vascular Endothelial Growth Factor (VEGF) (Miquerol et al., 1999), Ahnak (Kingsley et al., 2001; Downs et al., 2002), and even T (Downs et al., 2009), their role in mesothelium is unclear.

On the basis of these observations, we reasoned that allantoic mesothelium might exhibit regional differences reflective of differential mesothelial function, for example, interaction with surrounding tissues and/or uptake of materials from the exocoelom. Several decades ago, biotinylated dextran amine (BDA) had been introduced into the experimental cell biological repertoire to trace the anterograde pathway in neuronal cells (Veenman et al., 1992). Although BDAs have not been applied to the rodent yolk sac or allantois, similar tracer molecules have been used to investigate the endocytic properties of rodent yolk sac endoderm (Beck et al., 1967; King and Enders, 1970). Thus, to a first approximation, BDAs would enable us, in combination with systematic morphological assessment, to discover whether the murine mesothelium functioned as a homogeneous cell population or whether any regional differences might be revealed.

The presence of regional differences in permeability could then be explored by molecular analyses. Polarized epithelial cells are circumscribed at the apicolateral margins by three morphologically distinct intercellular junctions: occludens or tight junctions, adherens junctions and spot desmosomes. Together, these form what has come to be known as the apical junctional complex (Farquhar and Palade, 1963). Tight and adherens junctions play major roles in intercellular permeability and intracellular signaling (Fanning and Anderson,

2009). The mechanisms by which these junctions are created and interact are complex and largely obscure, and may vary with epithelial type (Steed et al., 2010). Nevertheless, several proteins have emerged as major participants, including zonula occludens-1 (ZO-1), afadin (AF-6), and Epithelial-cadherin (E-cadherin). ZO-1 is a member of the MAGUK (membrane-associated guanylate kinase homologs) family with binding domains to adherens, tight junction proteins and the actin cytoskeleton (Harstock and Nelson, 2008). E-cadherin, a single-pass, transmembrane glycoprotein that belongs to the classical cadherin family of Ca²⁺-dependent adhesion proteins, sometimes precedes the appearance of ZO-1 in the genesis of tight junctions (Takai and Nakanishi, 2003). Afadin, in whose absence the allantois does not form (Ikeda et al., 1999), plays major roles in the function of adherens and tight junctions (Mandai et al., 1997; Yokoyama et al., 2001; Takai and Nakanishi, 2003).

Given that the rodent allantois is thought to lack an endodermal component while most mammalian species have one (Mossman, 1987), we initiated a systematic investigation into allantoic mesothelium that might shed light on its biological activities, paying particular attention to cell morphology, the gross relationship between cells, cell packing, intracellular ultrastructure, permeability, and the molecular identity of junctional complexes. The implications of our findings are discussed with respect to morphogenesis of the chorio-allantoic placenta, allantoic vascularization, vascular patterning, and hematopoiesis.

MATERIALS AND METHODS

Mouse Strains, Animal Husbandry, Dissections, and Staging

Care of animals was in accord with institutional guidelines. Unless otherwise indicated, standard F2 embryological material was obtained by intercrossing inbred hybrids (B6CBAF1/J) (Jackson Laboratory, Bar Harbor, ME) (Downs, 2006). For mating, single estrous females were selected (Champlin et al., 1973) and placed with individual stud males just before the lights went off (13.00/1.00 or 21.00/9.00 lights off/lights on), and copulation plugs were identified up to 12 h later. Dissection, whole embryo culture, and staging were as previously described (Downs and Davies, 1993; Downs, 2006). Focus was on the earliest phase of allantoic development, namely appearance of the allantoic bud and bud elongation through the exocoelom, when the allantois is surrounded by exocoelomic fluid over all but its basal region, which is continuous with the embryo (Early Bud, EB, stage, ~7.25 days postcoitum, dpc - 6-8-somite pairs, -s; ~8.5 dpc). During this timeperiod, mouse conceptuses contain three cavities: amniotic, exocoelomic, and ectoplacental (Snell and Stevens, 1966); the latter of which begins to occlude at the head-fold stages (Uy et al., 2002). During dissection, care was taken not to deflate the amniotic and exocoelomic cavities, the hydrostatic pressure of which appeared to increase over time. Consequently, as the conceptus was divested of its deciduum and Reichert's membrane was reflected, the visceral yolk sac expanded, possibly releasing the allantois from contact with adjacent amnion and visceral yolk sac (see Results). In three experiments, conceptuses remained within their decidua at 5.0 dpc.

Intercellular Passage of BDAs

Dextran is a hydrophilic polysaccharide characterized by its moderate to high molecular weight, good water solubility, and low toxicity. Because of their uncommon poly-(α -D-1,6-glucose) linkages, which render them resistant to cleavage by most endogenous cellular glycosidases, they are biologically inert (Molecular Probes, Publication MP01800, 5 April 2006). BDAs have been used in a wide variety of cellular characterizations, including fate mapping, cell permeability, and intercellular communication (Reiner et al., 2000). As it had been shown to exhibit numerous microvilli, endocytic vesicles, and tight junctions at 7–11 dpc (Haar and Ackerman, 1971), the visceral yolk sac served as an internal control throughout these studies. Moreover, in other rodent species, visceral yolk sac endoderm exhibited the properties of an absorptive epithelium that limits the passage of large molecules into the paracellular space by virtue of its tight junctions (Beck et al., 1967; King and Enders, 1970). Thus, to observe the behavior of BDA passage in a well-described epithelium, we first exposed the outer layer of extraembryonic visceral endoderm of dissected intact conceptuses to BDA (Molecular Probes, Carlsbad, CA) of low (3,000; D7135; 1 experiment: LB (1), EHF (2), LHF (2), 2-s (1), 3-s (2), and 4-s (1) stages) and high (10,000; D1956; 2 experiments: EHF (1), 3-s (3), 4-s (1), and 5-s (1) stages) molecular weights (MW) at working solutions of 1 mg/ml dissection medium (Downs, 2006) (BDA 3,000) or 0.5 mg/ml (BDA 10,000), which were well below the maximum solubility of these conjugates (Molecular Probes, Publication MP01800, 5 April 2006). All BDA-exposed conceptuses were incubated at room temperature for 15 min, as signal intensity did not perceptibly increase thereafter (up to 30 min incubation, data not shown). BDA was lysine-fixable, i.e., lysine was incorporated into the dextran conjugate to permit fixation *in situ* with aldehydes for analysis. Thus, afterward, conceptuses were rinsed, fixed (Bouin's fluid, 2 h, 4°C), and prepared for embedding in paraffin wax (Downs, 2002). After sectioning (6- μ m thickness) and dewaxing, specimens were stained as described for immunohistochemistry (IHC) (Inman and Downs, 2006a) but omitting antibodies and using only an avidin-biotinylated horseradish peroxidase (HRP) (Elite ABC, Vector Laboratories, Burlingame, CA) procedure, followed by standard diaminobenzidine (DAB, liquid, Dako North America, Carpinteria, CA) reaction. We found that while BDA 10,000 was clearly visible in the apical aspect of yolk sac endoderm, BDA 3,000 was weak. In fact, BDA 3,000 was typically less brown than BDA 10,000 in all experimental conceptuses. We attribute this difference to the reduced number of moles biotin/mole dextran (0.7 moles for BDA 3,000 versus 1.1 moles for BDA 10,000). These, and all yolk sac control conceptuses in which BDAs were omitted (one experiment, stages: 1-s (1), 2-s (1), and 4-s (1)) were incubated for 15 min at room temperature alongside exocoelom-injected controls and processed as described above. All control conceptuses lacking BDA were negative for background staining.

To discover the permeability of allantoic mesothelium, at least three specimens per stage (EB; Late Bud, LB; Early, Late Headfold, EHF, LHF; 1-, 2-, 3-, 4-, and -5-s) were exposed to BDA 3,000 and BDA 10,000. Each type of BDA was systematically introduced into the exocoelom via a mouth-held microcapillary (~60 μ m, inner diameter). The volume of BDA injected was based on preliminary calculations of the volume of exocoelomic fluid. This was determined by placing individual embryos into a drop of phosphate-buffered saline (PBS; Sigma), the meniscus of which directly contacted the walls of the visceral yolk sac. A pulled microcapillary (inner diameter, ~1 μ m) was then used to puncture the visceral yolk sac and withdraw exocoelomic fluid from each embryo while a pair of forceps placed along the edge of the conceptus stabilized it during this procedure. For each stage, fluid was pooled into a small tube, quantified and the average volume of exocoelomic fluid was calculated: EHF, 0.17 μ l exocoelomic fluid ($N = 17$ specimens); 1-s, 0.24 μ l ($N = 4$); 2-s, 0.34 μ l ($N = 5$); 3-s, 0.14 μ l ($N = 7$); and 5-s, 0.26 μ l ($N = 8$). For the BDA injections, the content of the exocoelom was thus withdrawn with a similar fine hand-pulled pipette and replaced

with ~0.4 μ l of BDA. In addition, a limited number of somite-stage conceptuses were exposed to BDA 500,000 (D7142; 2 experiments: EHF (1), LHF (2), 1-s (1), 2-s (2), and 3-s (4)).

Histology and Immunostaining

For histological appreciation of the mesothelial surface, both paraffin- and plastic-embedded material was used. Paraffin sections were cut to a thickness of 6 μ m, processed, and counterstained in hematoxylin and eosin, as previously described (Downs et al., 1998); the following numbers of conceptuses were examined: EB (6), LB (7), LB/EHF (8), EHF (14), LHF (7), 1-s (6), 2-s (2), 3-s (16), 4-s (12), 5-s (8), 6-s (8), 7-s (7), and 8-s (4). Plastic material was cut to a thickness of either 1 μ m (laboratory of A.C.E.) or 3 μ m (laboratory of K.M.D.) and counterstained in toluidine blue, as previously described (Enders et al., 2006); the number of specimens examined in plastic was: EB (4), LB (6), LB/EHF (4), EHF (11), LHF (3), 1-s (6), 2-s (4), 3-s (7), 4-s (2), and 5-s (3). In addition, we examined paraffin-embedded specimens from two previously published protein localization papers that spanned the same stages and for which many conceptuses were available for each stage (Downs, 2008; Downs et al., 2009).

Immunohistochemistry (IHC) for afadin (AF-6; Abcam, Cambridge, MA; Ab11337; rabbit polyclonal; 0.9 mg/ml) was used at a dilution of 1/750; afadin IHC was carried out in both histological sections on Bouin's fixed material as previously described (Inman and Downs, 2006a), and in whole mount prepared material (Downs, 2008). For 5.0 dpc decidua and their conceptuses, fixation and immunostaining were carried out in paraformaldehyde-fixed and sectioned material as described in Downs et al. (1998). All other IHC was carried out in whole mount-prepared material alone. Anti-E-cadherin (Santa Cruz Biotechnologies, SCBT, Santa Cruz, CA; SC-59778; rat monoclonal; 0.2 mg/ml) and anti-ZO-1 (SC-8146; goat polyclonal; 0.2 mg/ml) were used at dilutions of 1/50-to-1/100, and anti-alpha-4 integrin (SCBT; SC-2042; goat polyclonal; 0.2 mg/ml) was used at dilutions of 1/75-1/100. Controls for the specificity of ZO-1 immunostaining in mouse gastrulae were carried out on 4-5-s stage conceptuses as follows: (i) minus antibody, (ii) prebinding ZO-1 antibody with its cognate control peptide (SC-8146P) in a ratio of 1:10 and 1:20 times the antibody concentration for 8 h at 4°C, (iii) antibody alone but held at 4°C for 8 h, and (iv) fresh antibody. In addition, immunostaining whole decidua at 5.0 dpc revealed ZO-1 staining in decidual cells around the conceptus, as previously described (Paria et al., 1999). As no control peptide was available for either E-cadherin or afadin, minus antibody controls alone were used at the 4-6-s stages. Controls for anti-alpha-4-integrin were previously reported (Downs, 2002). For all immunostained sections, detection of specific proteins was indicated by dark brown color.

Transmission and Scanning Electron Microscopy

Transmission electron microscopy (TEM) was carried out as previously described (Downs et al., 2004; Enders et al., 2006; Downs et al., 2009); the numbers of specimens examined here were: EB (4); LB (5); LB/EHF (2); EHF (7); LHF (3); 1-s (5); 2-s (4); 3-s (5); 4-s (2); and 5-s (3). Results were interpreted independently in the laboratories of A.C.E. and K.M.D. Allantoises were examined especially for tight junction profiles, comparing candidates against the extraembryonic visceral endoderm of the yolk sac (Farquhar and Palade, 1963; Haar and Ackerman, 1971) in the same section wherever possible.

For scanning electron microscopy (SEM), three litters (~8.5 dpc) were dissected as described above. 18 conceptuses were fixed and maintained in Sorensen's buffer (4% paraformaldehyde/1% glutaraldehyde/0.1 M phosphate) for 10 h at 4°C, rinsed in 0.1 M phosphate buffer, in which most of the yolk sac was removed. Conceptuses were then dehydrated in an increasing series of ethanols, then cryofractured and dried using the

critical point method. The next day, specimens were mounted and sputter-coated in gold at 16.0–18.7 Pa and a current of 30 A for 2 min. Of these, two conceptuses were adequately prepared, viewed and photographed in a Hitachi S-570 LaB₆ Scanning Electron Microscope, maintained by the Biological and Biomaterials Preparation, Imaging and Characterization (BBPIC) Laboratory (Department of Animal Sciences, University of Wisconsin-Madison).

RESULTS

Allantoic Mesothelium Exhibits Distinct Morphological Properties Over Time

The morphology of the allantoic mesothelium and its relationship to surrounding tissues was examined systematically over time by light microscopy. The surface of bud-stage (EB, LB) mesothelium was highly variable. Although the nascent allantoic bud could exhibit a mostly squamous surface (data not shown), most specimens showed an irregular contour in which cells varied from squamous to tall polygonal where just a portion of the apical surface contacted the exocoelom (Fig. 1A,B). Many outer cells were connected with neighboring surface cells either in ad hoc manner or were not connected to them at all in individual sections.

By the EHF stage, increasing intercellular space was observed between distal core cells relative to the proximal region (Fig. 1C,D). Many, but not all, distal mesothelial cells appeared to be flattening, whereas proximal mesothelium remained polygonal. In some paraffin-prepared specimens, the exocoelom had not expanded upon reflexion of Reichert's membrane, possibly because the exocoelom had not yet enlarged or because the walls of the exocoelom had been imperceptibly nicked; whatever the reason, the allantois could be visualized in these specimens growing in a directed manner toward the chorion between the amnion and yolk sac (Fig. 1E), suggesting that the allantois may communicate directly with nearby tissues via its mesothelium.

By the LHF stage (Fig. 1F–I), distal mesothelium was generally squamous, though it also included elongated cells whose apex reached the free surface (Fig. 1F). Proximal mesothelium was polygonal-to-cuboidal in shape (Fig. 1G). "Ventral cuboidal mesothelium" ("VCM") overlay the previously described allantoic growth center, the ACD, and extended for a short distance onto adjacent visceral yolk sac endoderm, forming a "V"-shaped structure (Fig. 1H). By contrast, "dorsal cuboidal mesothelium" (DCM), on the opposite proximal surface of the allantois, while also cuboidal, exhibited a "horseshoe" shape and was continuous with the amnion (Fig. 1I).

By 4-s, both the "vessel of confluence" (VOC), or site of amalgamation of the major arterial systems in the conceptus, and the hindgut invagination invariably appeared within the midline, beneath the bend of the VCM's V-shape, in register with

the primitive streak along the embryonic antero-posterior (A-P) body axis (Fig. 1J). In addition, although "blebs" were observed on the surface of the allantois from headfold stages on, they were particularly prominent in the inbred hybrid mouse strain used in this study by 4-s, appearing as circles of flattened cells enclosing a small cluster of roundish ones (e.g., Fig. 1K). In addition, the DCM region invariably presented as large protrusions of irregular contour that contacted the amnion (Fig. 1L) and remained so over the next stages. Distal mesothelium was still generally squamous but punctuated with occasional scattered elongated cells (Fig. 1M).

By 8-s, just after fusion but prior to tail rotation, the hindgut had deeply invaginated into the embryo, and the VCM appeared to lengthen over the VOC. As the latter elongated, appearing to become the omphalomesenteric artery, the VCM merged with the caudal embryonic primary body fold (Fig. 1N). Similarly, the DCM was becoming continuous with the dorsal epithelium of the embryo (Fig. 1N).

The irregular contours of allantoic mesothelium were supported by SEM analysis (Fig. 2). At 4-s, the VCM appeared relatively smooth, whereas the DCM exhibited several large blebs; the distal half of the allantois showed an irregular surface. At 8-s, the distal half of the allantois contained many prominent blebs (Fig. 2D,E), while the transitional zone (Fig. 2F) provided a direct comparison between the blebbed distal region and the proximal region bearing the VCM (Fig. 2G). Thus, by headfold stages, distal and proximal mesothelium revealed regional morphological differences, with distal mesothelium generally squamous and proximal mesothelium generally cuboidal.

Differential Permeability of Allantoic Mesothelium to BDA

At all stages, high-MW BDA (BDA 10,000) was associated with the apical surface of the yolk sac; some regions were darker than others, but the BDA did not obviously penetrate the spaces between the cells (Fig. 3A,B). While TEM was not used to assess the precise whereabouts of high-MW BDA on the surface of the yolk sac, that BDA was not obvious between cells or beneath yolk sac endoderm suggested that it did not diffuse between cells. Thus, these results are consistent with an epithelium that does not readily allow the passage of molecules through its paracellular pathway.

By contrast, yolk sacs exposed to low-MW BDA (BDA 3,000) exhibited a low but detectable signal on their surface (Fig. 3C). Given the fewer number of biotin molecules associated with the low-MW BDA (see Materials and Methods), and the limited number of BDA molecules that can be taken up by

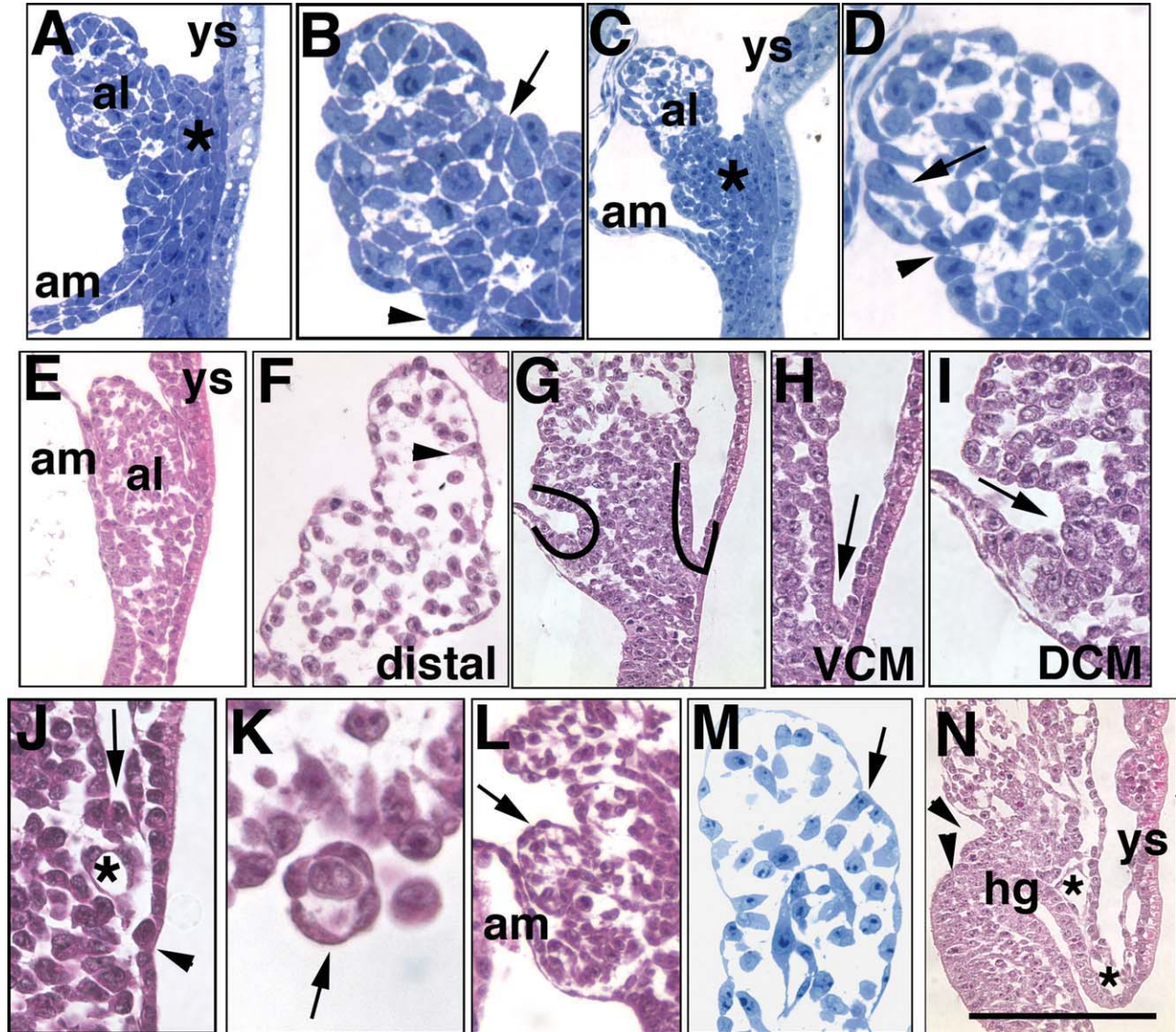


Fig. 1. Analysis of the allantoic surface (allantoic bud stages 8-s). Light microscopy (LM). Plastic- (A–D, M) and paraffin- (E–L, N) embedded histological sections. For all sagittal allantoic profiles, distal is toward the chorion, and proximal is toward the embryo. (A, B) Late Bud (LB)-stage. Low- (A) and high- (B) magnification of the allantois (al) and its associated visceral yolk sac (ys) and amnion (am). Asterisk, Allantoic Core Domain (ACD). Arrow, examples of long polygonal mesothelial cells whose apices reach the surface; arrowhead, a mesothelial cell with few or no intercellular contact points. (C, D, E) Early Headfold (EHF) stage. Low- (C) and high- (D) magnification images. Arrow and arrowheads as in (A, B). (E) Allantoic elongation appears to be directed toward chorion by expansion of the amnion and buttressing by the visceral yolk sac, demonstrating the potential intimacy between allantoic mesothelium and the adjacent amnion and yolk sac. (F–I) Late Headfold (LHF) stage. (F) Distal mesothelium shows abundant squamous cells with the insertion of occasional elongated polygonal ones (arrowhead). (G) Lines delineate crescent-shaped dorsal cuboidal mesothelium (DCM; left) and V-shaped ventral cuboidal mesothelium (VCM; right). (H) VCM. Arrow indicates the “vertex” of this V-shaped structure, and its association with both the allantois and yolk sac endoderm. (I) DCM. Arrow indicates the concave-area formed by the DCM. (J–M) 4-somite pairs (s). (J) VCM and associated vessel of confluence (VOC; asterisk). (K) Allantoic bleb (arrow). (L) Large dorsal bleb (arrow) in region of DCM associated with amnion. (M) Distal allantois shows abundant squamous cells with an occasional polygonal one (arrow). (N) 8-s. The VCM appears to have elongated over the VOC, which appears to have elongated over the hindgut (hg), thereby forming the omphalomesenteric artery whose ends are indicated by asterisks. Pair of arrowheads points to DCM and its dorsal continuity with the embryonic body wall prior to tail turning. All scale bars in this, and all other figures, are approximate to within 7 μ m. Scale bar in (N) = 100 μ m (L); 75 μ m (K); 50 μ m (B, D, J); 35 μ m (E, H, I); 25 μ m (A, F, M); 17 μ m (C, G, N). [Color figure can be viewed in the online issue, which is available at wileyonlinelibrary.com.]

yolk sac endocytosis, detection of uptake and/or association with the microvilli may have been at the threshold of streptavidin/horseradish peroxidase visualization used here.

With these profiles in hand, BDAs were then introduced into the exocoelom of mouse conceptuses at stages representing 2–4 h intervals, from the time of the appearance of the allantoic bud

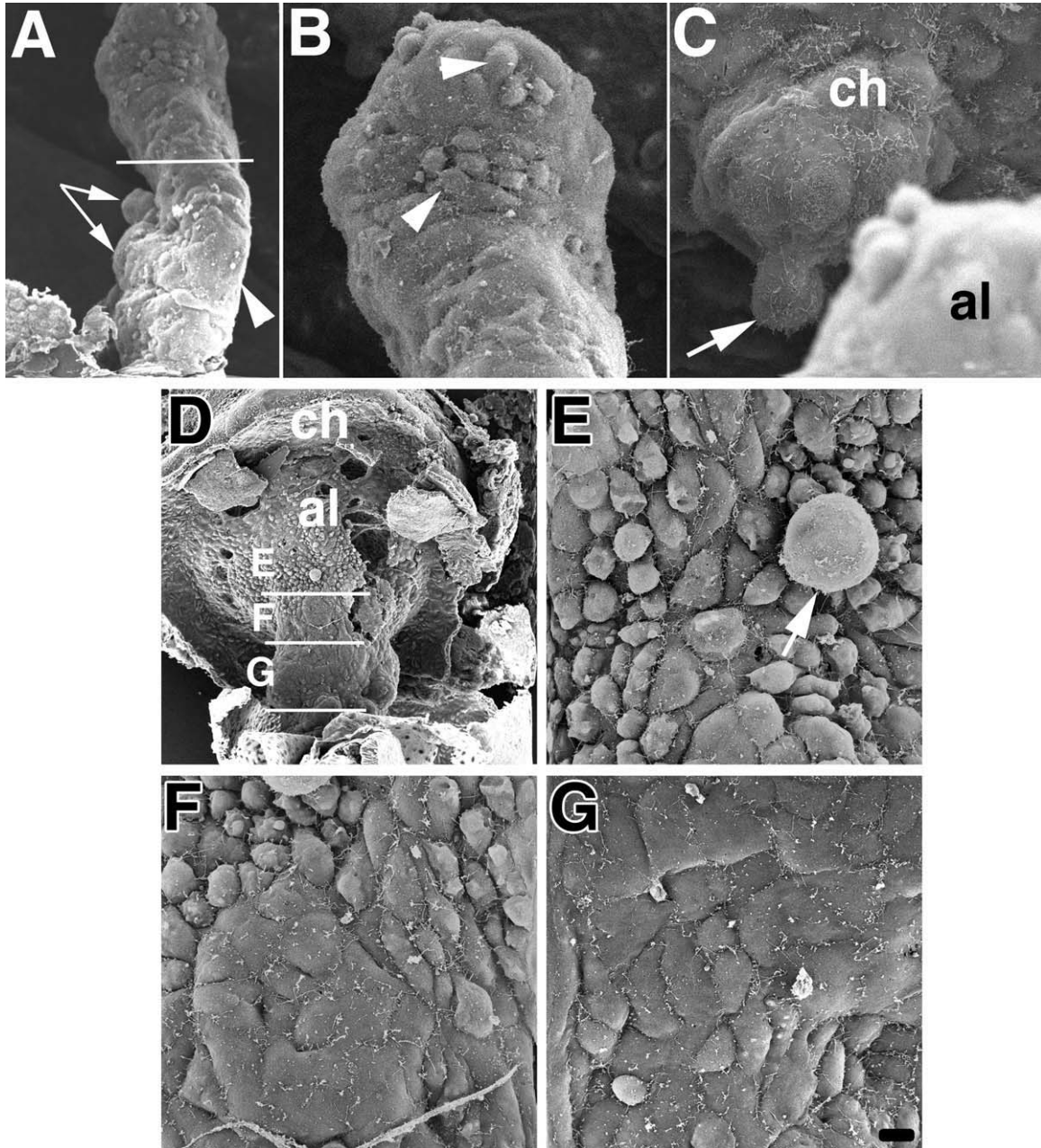


Fig. 2. The allantoic surface at 4- and 8-s stages. Scanning electron microscopy (SEM). (A–C) 4-s stage. (A) Allantois viewed obliquely from the ventral surface (arrowhead); horizontal white bar delineates the lower VCM region from the upper distal region; paired arrows, DCM region showing large dorsal protrusions normally extending toward the amnion (see Fig. 1L). Distal region above horizontal bar is shown at higher magnification in (B), which highlights the irregular allantoic surface, with protruding mesothelial cells (arrowheads). (C) Blebs on the chorion (ch) at the site of allantoic fusion (Downs, 2002). The distal tip of the allantois (al) is in the foreground. (D–G) 8-s stage. (D) Allantois has fused with the chorion. Horizontal bars delineate levels shown at higher magnifications in panels E–G. (E) Arrowhead highlights a large bleb in the distal allantoic region. (F) Mid-allantoic region between distal region and relatively smooth proximal region. (G) Proximal VCM region. Scale bar in (G) = 115 μ m (A, D); 20 μ m (C); 15 μ m (B, E–G).

(~7.25 dpc) through just before the elongated allantois's fusion with the chorion (5-s, ~8.25 dpc). The exocoelom surrounded all but the proximalmost part of the allantois. "No dextran" controls were negative (compare Fig. 3D,E), confirming the specificity of the reagents used here.

At bud stages, allantoic mesothelium was permeable to the passage of low-MW BDAs (Fig. 3F,G). Low-MW BDA was associated with both the outer and inner cell populations of the allantois, appearing to pass easily between mesothelial cells. By contrast, bud-stage allantoises were impermeable to

passage of high-MW BDAs (Fig. 3H). In these, high-MW BDA accumulated both on the surface of allantoic mesothelium, as well as between these outer cells, but did not progress into the allantoic core.

By headfold stages, the overall permeability of the allantoic surface had changed and

become regionally distinct. Distal mesothelium (here defined as the distal two-thirds of the allantois) was highly permeable and remained so at all stages thereafter to both low- and high-MW BDA (Fig. 3I,J,P,Q). By contrast, pas- sage of BDA into the proximal (here defined as

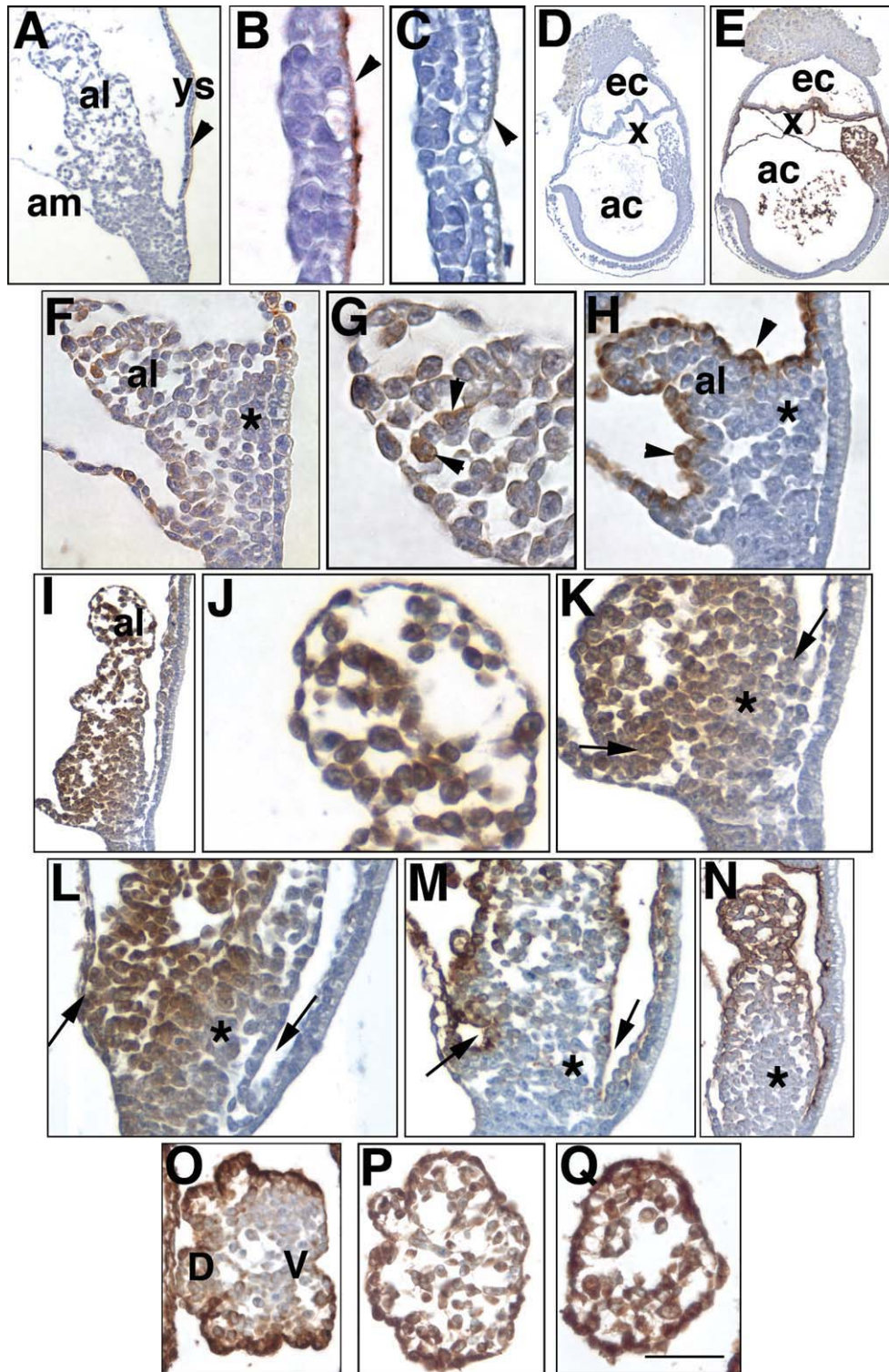


Figure 3.

the proximal one-third of the allantois) core appeared to be less facile. In particular, the VCM, which overlay the ACD, appeared to be impermeable to BDA challenge at all stages (Fig. 3I,K–M): low-MW BDA was found only faintly on the surface of the VCM and underlying cells (Fig. 3I,K,L), whereas high-MW BDA was accumulated at the VCMs cellular surface and rarely penetrated into the underlying allantoic core (Fig. 3M,O). By contrast, the DCM was permeable to low-MW BDAs, gaining access to the underlying cells (Fig. 3I,K,L), whereas high-MW BDAs were largely inhibited from entering (Fig. 3M,O). These findings are summarized graphically in Fig. 4 by a permeability index (PI).

The PI assumed that entry of BDAs into the allantoic core was limited to lateral, rather than longitudinal, diffusion. To test this hypothesis, we exposed allantoises to BDA 500,000 in a limited number of experiments. BDA 500,000 was associated with distal mesothelial cells and the underlying distal core but had not diffused into the proximal core region (Fig. 3N). In the proximal regions, BDA 500,000 remained associated with the cell surface but did not penetrate to underlying core cells (Fig. 3N). Together, results of BDA challenge suggest that allantoic mesothelium is regionally differentially permeable and that underlying core cells may be intimately regionally related to their associated mesothelium.

Localization of ZO-1 and E-Cadherin to Allantoic Mesothelium

Variable permeability of distal mesothelium and the VCM appeared to correlate with cell shape, with generally squamous distal mesothelium permeable to BDA and cuboidal VCM impermeable. However, the DCM, which was morphologically

similar to the VCM, was variably permeable, suggesting that mechanisms other than cell shape regulated permeability.

The apical surface of the yolk sac endoderm was robustly ZO-1-positive, forming an intensely staining continuum there (Fig. 5A–D,F,G). In addition, ZO-1 was found within that visceral endoderm which overlies the allantois (Fig. 5A–D), previously referred to as “allantois-associated extraembryonic visceral endoderm,” or the AX, and whose morphological properties were previously shown to be intermediate between those of yolk sac endoderm and visceral embryonic endoderm (Downs et al., 2009). ZO-1 was also found in embryonic visceral endoderm (data not shown). By contrast, ZO-1 was not particularly robust in the allantois at any stage (Fig. 5), being found faintly in both outer and inner cells. Within the core of the allantois, ZO-1 appeared punctate and scattered throughout (e.g., Fig. 5A–G). By contrast, the only part of the mesothelium where ZO-1 formed the most convincing continuum of, albeit weakly staining cells, was in the presumptive bud-stage VCM (Fig. 5B) and in the VCM visible by headfold stages (Fig. 5C,D,F,G). Still, relative to the yolk sac, staining was weak. Specificity of the ZO-1 antibody was confirmed in the deciduum surrounding 5.0 dpc conceptuses (Fig. 5H), and further shown with prebinding of ZO-1 antibody with control peptide (Fig. 5I) and minus antibody controls (Fig. 5J).

E-cadherin was found robustly throughout the visceral endoderm, both extraembryonic (Fig. 6A), and embryonic, including the endoderm overlying the heart field (Fig. 6B), the apical surface of the neurectoderm, (Fig. 6B) and the ventral node (e.g., Fig. 6C) at all stages. E-cadherin was also found throughout the primitive streak, being most intense at the neural plate/allantoic bud stages but decreasing in intensity thereafter (data not shown). Within the allantois, E-cadherin localized

Fig. 3. Permeability of allantoic mesothelium as revealed by challenge with biotinylated dextran amines (BDA; brown color). LM. (A–C) Low-(A) and high-(B) magnification images of BDA 10,000 (“high” molecular weight, MW) in posterior yolk sac endoderm. Although the intensity of BDA association with the yolk sac varied from region to region, most, if not all cells of the yolk sac visceral endoderm were associated with this high-MW BDA (arrowheads). (C) BDA 3000 (“low” MW) in posterior yolk sac endoderm; arrowhead indicates areas of faint staining. (D–E) 4-s stage controls indicating three major cavities in the conceptus, amniotic (ac), exocoelomic (x), and ectoplacental (ec). “No dextran” control (D), and high-MW dextran injected into the exocoelom (E). Brown stain in amniotic cavity (ac) suggests that high-MW BDA might diffuse through amnion into the amniotic cavity (Daane and Downs, unpublished data). (F–G) LB stage, low-MW BDA 3,000 at low- (F) and high- (G) magnifications. Asterisk indicates the ACD region; arrowheads indicate BDA-positive core allantoic cells. (H) LB stage, high-MW BDA 10,000. Arrowhead indicates BDA on and around mesothelial cells, with little-to-no penetration into the allantoic core. (I–K) LHF stage. Low- (I) and high- (J, K) magnifications of the whole allantois (I), distal region (J), and proximal region (K). Left arrow in (K) indicates region of DCM and right arrow that of the VCM. Asterisks indicate location of ACD. (L) 5-s stage, low-MW BDA 3,000, proximal allantoic region; left and right arrows, asterisk, as in (K). (M) 5-s stage, high-MW BDA 10,000, left and right arrowheads, asterisk, as in (K, L). (N) 4-s stage, BDA 500,000. Note high concentration of BDA on distal mesothelial cells with penetration of BDA into the distal region, while BDA is less abundant on proximal surface, with little-to-no penetration into the core, providing supporting evidence for regionalization of allantoic mesothelium by these stages. (O–Q) 5-s stage, high-MW BDA 10,000, transverse sections through proximal (D, DCM region; V, VCM region; lower one-third (O), mid- (middle third) (P), and distal (distal third) (Q) allantoic regions. Scale bar in (Q) = 100 μ m (C, G, I, L, N); 115 μ m (B); 150 μ m (D); 165 μ m (E); 200 μ m (M); 250 μ m (K); 340 μ m (A); 375 μ m (J); 65 μ m (H); 60 μ m (Q); 50 μ m (F, O); 40 μ m (P).

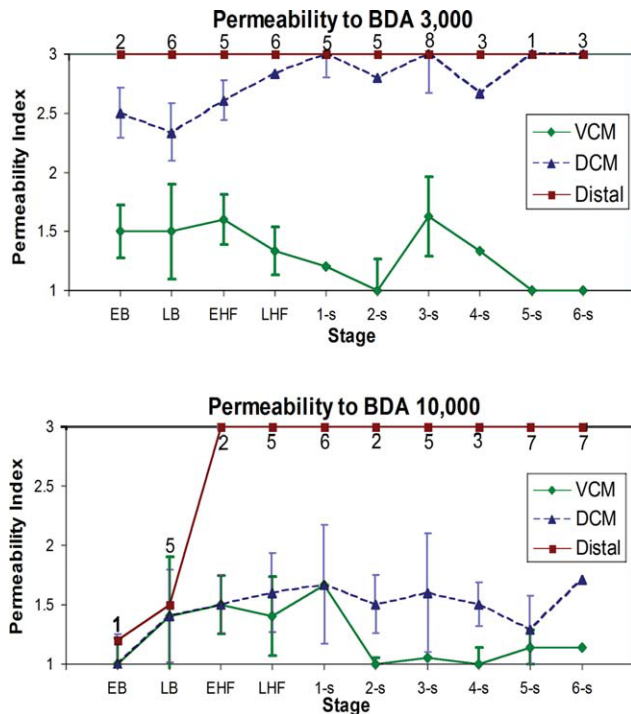


Fig. 4. BDA permeability index (PI). PI for three mesothelial regions, distal, VCM, and DCM. Scores ranged from 1 (impermeable, dextran located mesothelial surface only) to 3 (permeable, dextran spread throughout the core). A value of 2 was assigned if brown stain of BDA was observed only on cells immediately beneath the mesothelial surface. Sample sizes are indicated for each developmental stage. Error bars represent \pm standard error of the mean. [Color figure can be viewed in the online issue, which is available at wileyonlinelibrary.com.]

to the proximal inner core and extended through the allantoic midline (Fig. 6D–G) in a pattern that seemed, at least in part, to overlap that of the T-defined ACD. E-cadherin was also present in the AX at all stages (Fig. 6D–G). By 5-s, E-cadherin was no longer observed in the allantois (Fig. 6H,I) and resembled the minus antibody controls (Fig. 6J). The hindgut invagination, continuous with extraembryonic and embryonic visceral endoderm, was strongly E-cadherin positive (Fig. 6F–I,K).

Together, these data suggest that E-cadherin and ZO-1 do not overlap in allantoic mesothelium and thus do not cooperate in building and/or maintaining the outer surface of the allantois.

Transmission Electron Microscopy

In a previous study (Downs et al., 2004), the mesothelium of the allantois had been examined at a few incremental stages by TEM. Simple adhesion plaques and spot desmosomes were noted at all stages, though neither the distal nor proximal halves were favored. Only one example of a possible junctional complex was reported, at the early

bud (EB) stage, in which a putative tight junction, adherens junction, and spot desmosome were identified in the same plane of section (Fig. 4 in Downs et al., 2004).

On the basis of our permeability data, we systematically examined the allantoic mesothelium by TEM, comparing its profile with that of the yolk sac endoderm, an established epithelium. Cells of yolk sac endoderm exhibited abundant microvilli, coated vesicles of varying sizes, much rough endoplasmic reticulum, and many mitochondria (Fig. 7A). Individual endodermal cells were so closely packed and so highly interdigitated that intercellular boundaries were difficult to discern; when an apical intercellular junction was identified, it was always impossible to follow it to its nether reaches (e.g., Fig. 7A). Nevertheless, we occasionally identified provisional junctional complexes in the yolk sac endoderm (e.g., Fig. 7B,C) beneath which the cell membranes were highly interdigitated (Fig. 7C).

At bud stages, most outer allantoic cells were arranged in ad hoc manner with no continuity between them (Fig. 7D). The apical surface of these cells was irregular and scalloped (Fig. 7E–G). Intercellular contact between cells could either be minimal, involving one focal site (e.g., Fig. 7E), or more expansive, involving close contact between cells along their entire length (Fig. 7E–G). Bud-stage mesothelial cells exhibited few vesicles, some strands of rough endoplasmic reticulum, and abundant polyribosomes (Fig. 7E–G).

Close inspection revealed that, unlike the yolk sac, mesothelial cells were not interdigitating with each other at any stage. Thus, if junctional complexes were present, they should be detectable. We were not able to discern junctional complexes typical of an epithelium; rather, each contact point appeared as a simple adhesion junction, either a collection of poorly defined densities or more often, exhibiting a blanket stitch profile (e.g., Fig. 7H). Spot desmosomes were occasionally observed at all stages, with no preferred site of regional localization. At no stage was a clear basal lamina observed beneath the mesothelial cells by TEM.

At headfold through 5-s stages, outer distal mesothelial cells exhibited two profiles: some cells were still polygonal (Fig. 8A), with multiple intercellular contacts generally made near their apical surfaces, or, more often, cells were squamous, with single intercellular contact points between them (Fig. 8B). In addition, while distal cells displayed occasional vesicles (Fig. 8A), the majority of intracellular organelles appeared to be polyribosomes (not shown) with occasional strands of rough endoplasmic reticulum and mitochondria. By contrast,

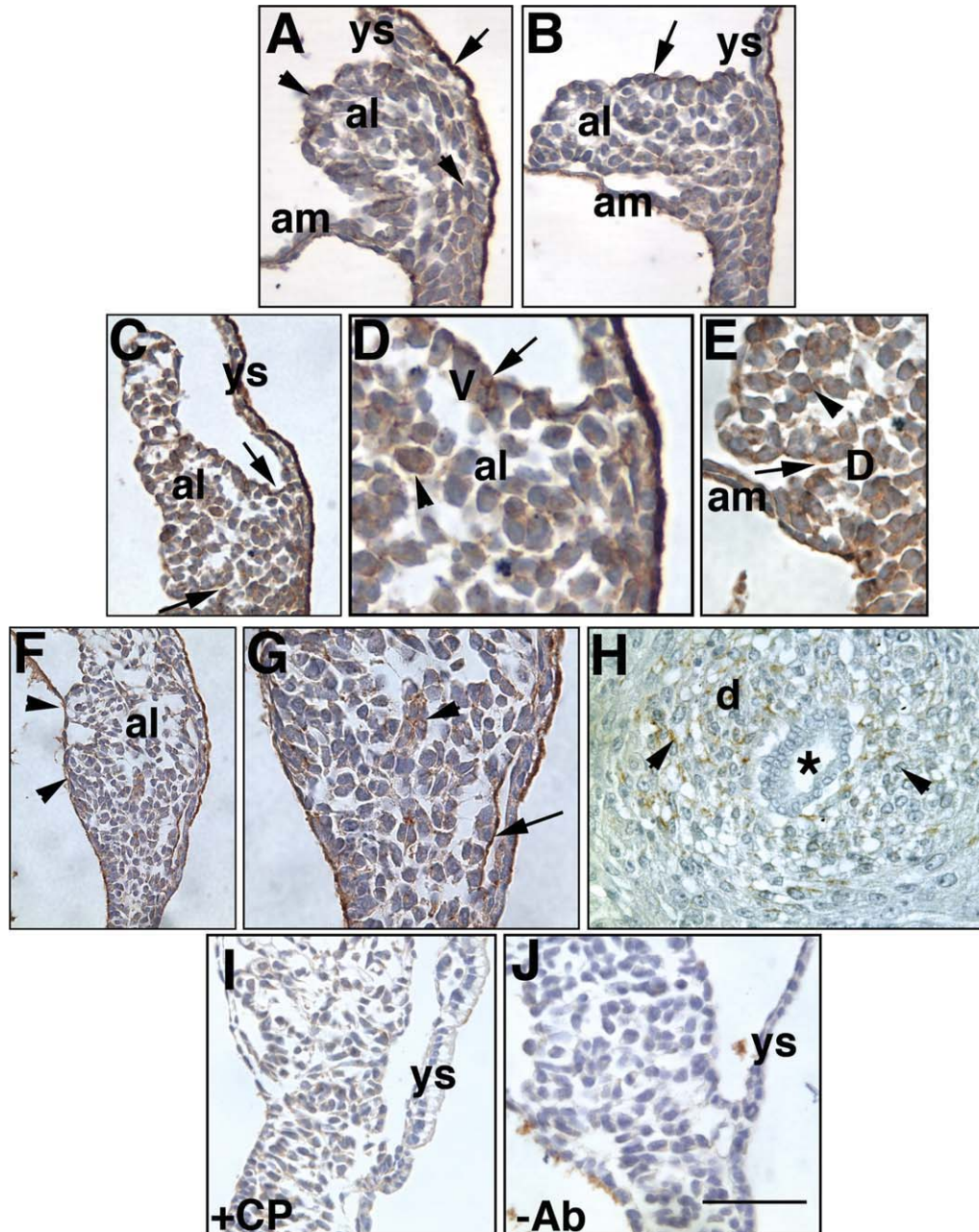


Fig. 5. Localization of Zonula occludens-1 (ZO-1) to visceral yolk sac endoderm and allantois. LM. (A) Early bud (EB) stage. Arrow, ZO-1 signal in yolk sac endoderm. Arrowheads, examples of ZO-1 signal on the surface of and within the allantois. (B) LB stage. Arrow, example of ZO-1 signal in presumptive VCM region. (C–E) LHF stage. Lower arrow, left, DCM region; upper arrow, right, VCM region. (D) Arrow, VCM region (V); arrowhead, ZO-1-positive allantoic core cell. (E) Arrow, DCM region (D) showing positive ZO-1 signal; arrowhead, ZO-1 within allantoic core. (F, G) 4-s stage. Low- (F) and high- (G) magnifications of an allantois growing between the amnion and the yolk sac; arrowheads indicate contact points between dorsal protrusions and amnion. (G) Higher magnification shows proximal allantoic region; arrowhead indicates a cluster of ZO-1 core cells; arrow indicates ZO-1 staining on VCM. (H) Positive control for ZO-1. Deciduum (d) surrounding conceptus (asterisk) at 5.0 days post-coitum (dpc) exhibits punctate ZO-1 staining (arrowheads). (I, J) Control conceptuses for control peptide (CP), 6-s (I) and minus antibody (-Ab), 5-s (J). See Materials and Methods. Scale bar in (J) = 50 μ m (A, B, G, J); 100 μ m (D); 75 μ m (E); 35 μ m (C, H, I); 25 μ m (F).

both cuboidal DCM and VCM cells made discrete intercellular contacts along their length, leaving wide gaps of intercellular space between them (Fig. 8C,D). They exhibited some vesicles (Fig. 8C) and

considerable rough endoplasmic reticulum (data not shown). Nuclei were irregularly shaped. Intercellular junctions were of the blanket stitch type (Fig. 8E,F), or somewhat poorly defined (Fig. 8F).

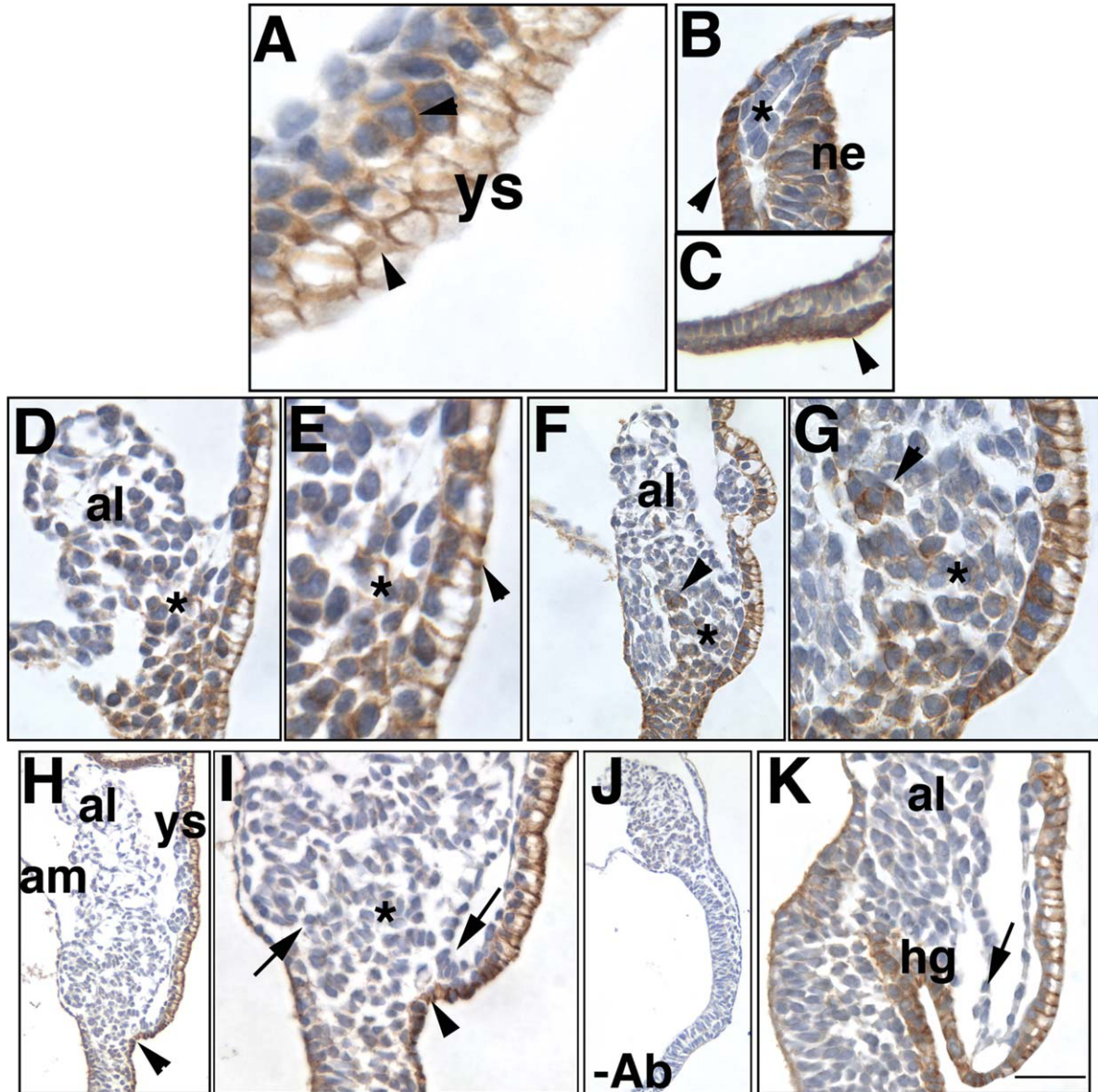


Fig. 6. Localization of Epithelial-cadherin (E-cadherin) to the allantois and other tissues. LM. (A) LB stage, visceral yolk sac endoderm (ys). Arrowheads point to examples of E-cadherin-positive cells. The outermost cells have been cut obliquely across the apex of the endoderm; because the apex is highly vacuolated, the cells appear as empty space. (B, C) EHF stage, same conceptus. (B) Asterisk, cardiac field. E-cadherin is not discernible. Arrowhead, notochord/endoderm and neuroectoderm (ne) are positive for E-cadherin. (C) Node, arrowhead, is positive for E-cadherin. (D, E) LB stage at low- (D) and high- (E) magnifications. Asterisk indicates the ACD region, which is E-cadherin positive. Arrowhead, example of positive cells in yolk sac endoderm. (F, G) EHF stage at low- (F) and high- (G) magnifications, showing E-cadherin-positive midline core cells (arrowheads), and ACD region (asterisks). (H, I) 5-s stage. E-cadherin is not discernible in the allantois, particularly its DCM (left arrow, I) and VCM (right arrow, I) but was strong in the endoderm of the hindgut invagination (arrowhead). Asterisk, ACD region. (J) 5-s stage. Minus antibody control. (K) 8-s stage. Arrow indicates the VCM; hg, hindgut. Scale bar in (K) = 100 μ m (G, H); 125 μ m (E); 150 μ m (A); 210 μ m (C); 85 μ m (B, J); 75 μ m (D); 60 μ m (I, K).

Finally, the cells of the allantoic blebs (Fig. 1K) looked identical to other mesothelial cells except that they formed spherical projections of cells connected by a few spot adhesion junctions surrounding a few central cells (Fig. 9). Their porosity to BDAs was similar to that of distal mesothelium, and they exhibited all of the other properties

described in this study for distal mesothelium (data not shown).

Together with results of IHC for ZO-1 and E-cadherin, these ultrastructural observations suggested that mature tight junctions are absent or rare on the surface of the allantois at all stages examined here.

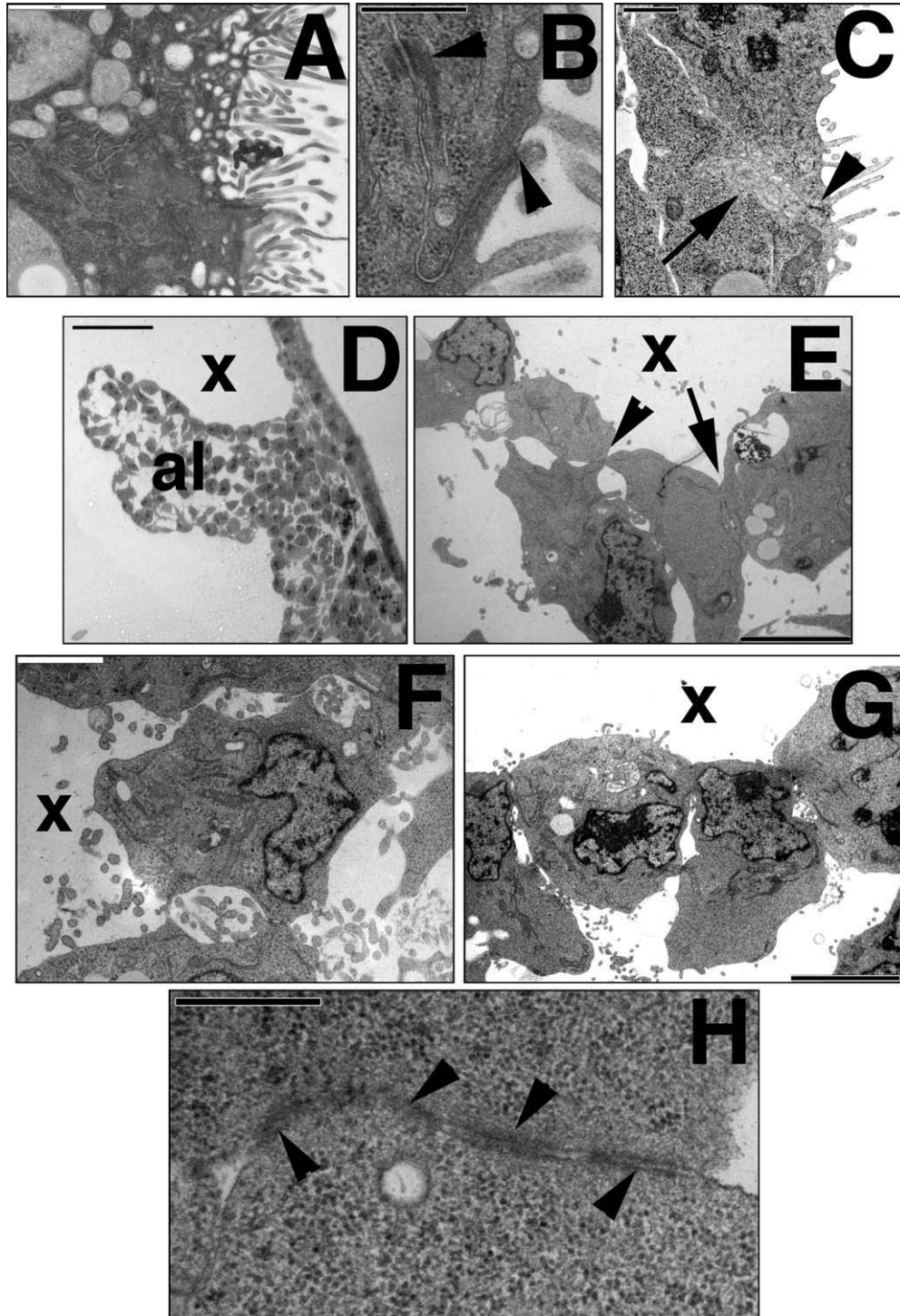


Fig. 7. Cell contacts and ultrastructure in allantoic bud stages. Transmission electron microscopy (TEM). (A–C) 3-s stage. Yolk sac endoderm. Overview of visceral yolk sac endoderm (A), showing numerous microvilli, vesicles, and abundant rough endoplasmic reticulum of two contiguous cells. Higher magnification (B) shows example of two contiguous cells sharing a potential junctional complex of a tight junction, adherens junction and a spot desmosome. Arrowheads indicate start and end of the junctional complex. (C) Two contiguous endodermal cells overlying the allantois, 1-s stage, showing interdigitation (arrow) between them, just beneath the junctional complex (arrowhead). (D–G) LB stage. Low magnification of the LB stage allantois (D); high magnification of the distal allantois (E) showing ad hoc contacts between cells (arrowhead indicates one focal site, arrow many focal sites between cells); DCM (F) and VCM (G). (H) EB stage. Example of a typical point of contact between two cells, in this case, within the DCM. Note the blanket stitch profile of the intercellular connections (arrowheads); this junctional profile was found between mesothelial cells in all regions at all stages. Scale bars in upper left or lower right panels = 2 μm (A, F); 500 nm (B, H); 600 nm (C); 50 μm (D); 5 μm (E, G).

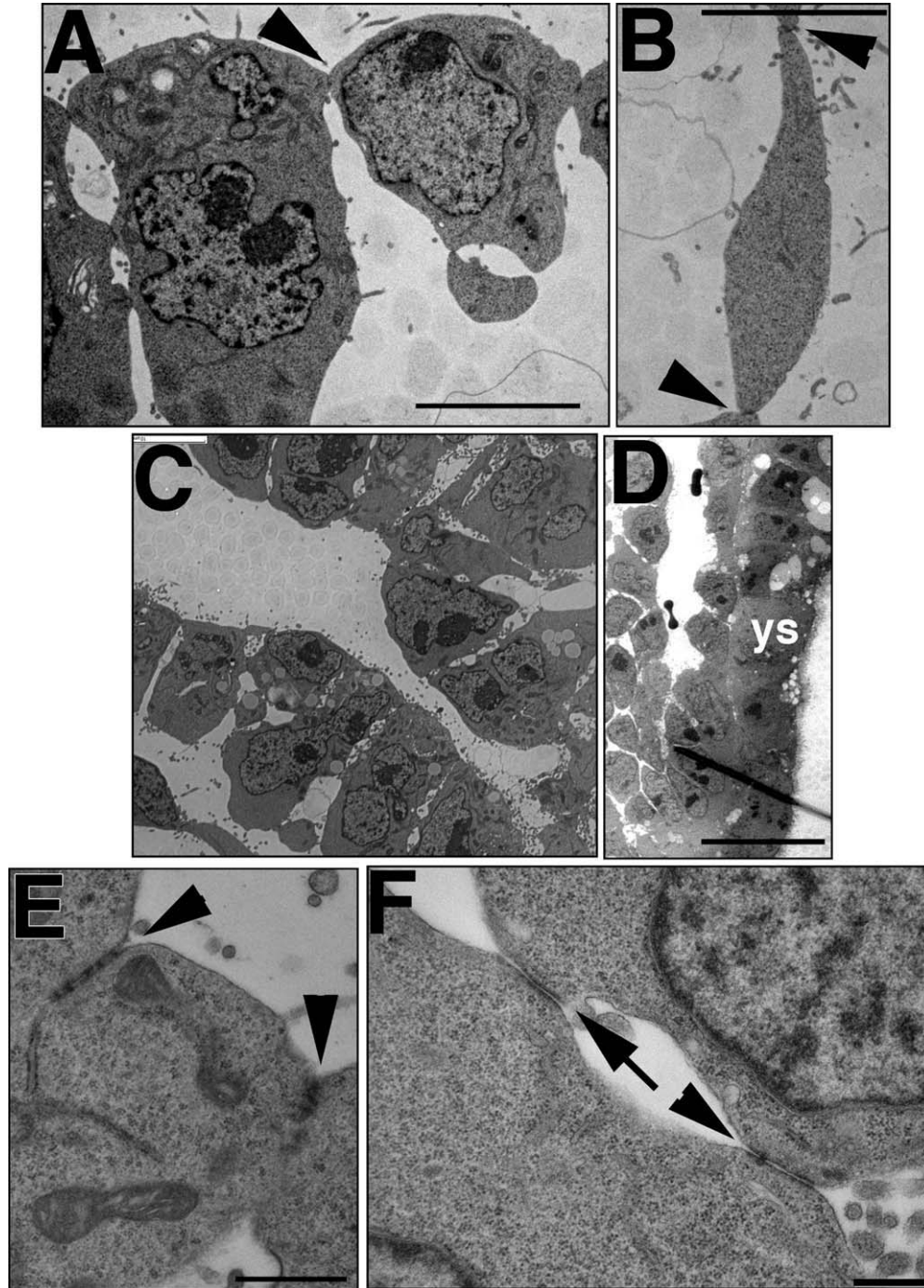


Fig. 8. Cell contacts and ultrastructure in headfold and early somite stages. TEM. (A, B) LHF stage, distal profiles of polygonal (A) and squamous (B) cells and their contacts (arrowheads). (C–F) 3-s stage. DCM (C), VCM (D), examples of similar blanket stitch adhesion junctions (arrowheads, E, F) or more poorly defined ones (arrow, F) in distal mesothelium (E) and VCM (F). Scale bars in panel corners = 5 μm (A, B); 10 μm (C); 20 μm (D); 1 μm (E); 500 nm (F).

Afadin and Alpha-4-Integrin Exhibit Distinct Regional Properties on VCM and DCM

The apical surface of yolk sac endoderm was positive for afadin at all stages, forming a robust continuum (Fig. 10). In bud stage allantoises, afadin levels

appeared to be strongest in mesothelium, but afadin was also found throughout core allantoic mesoderm (Fig. 10A). In addition to the visceral endoderm of the yolk sac, afadin localized to the AX.

By the headfold stages, afadin appeared as a continuous stripe on the surface of the VCM.

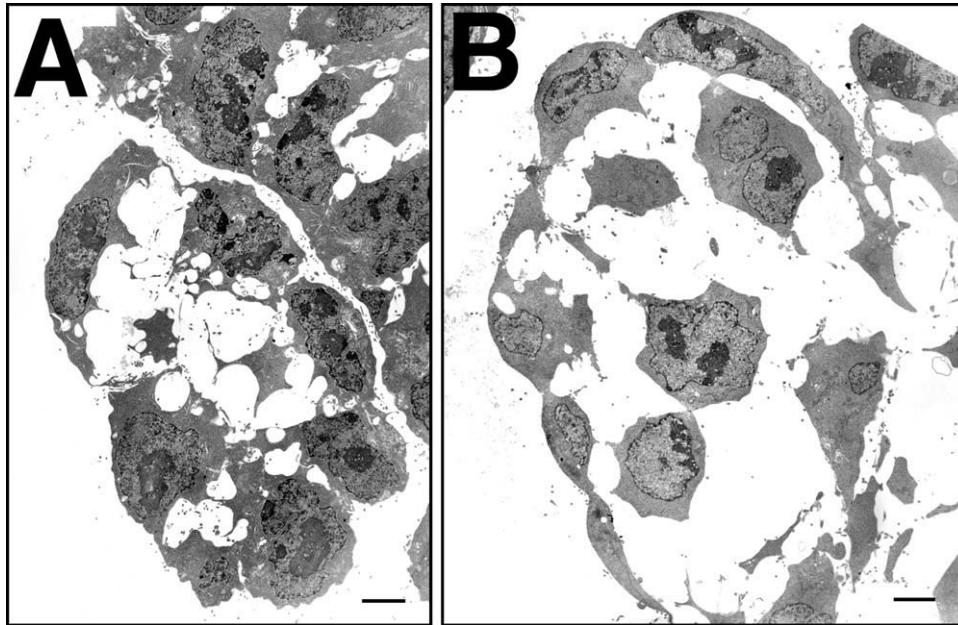


Fig. 9. Ultrastructure of allantoic blebs. (A) 2-s stage. An allantoic bleb composed of several mesothelial cells surrounding portions of more central cells. The communication with the allantois on the right has been cut off due to sectioning. (B) 5-somite stage. A distal bleb with several mesothelial cells surrounding several internal cells. The bleb loosely communicates with the allantois on the right. The relatively large amount of extracellular space is also characteristic of this later stage. Scale bars = 2.0 μm (A); 2.6 μm (B).

Within the DCM, staining was more diffuse and associated with underlying core cells and throughout the remainder of the allantois (Fig. 10B). These observations highlight the generally more regular positioning of the VCM vis-à-vis other allantoic cells. Although robust afadin persisted in the VCM and DCM throughout the timeperiod examined, it seemed to be strongest in the VCM by 4-s (Fig. 10C,D) where it appeared to surround VCM cells rather than be confined to the apex, as in the yolk sac and AX (Fig. 10C,D,G). Given that afadin was strongest at this stage, we used 4-s specimens to show specificity of antibody staining (compare Fig. 10E,F). At 6-s, afadin staining abruptly terminated within the yolk sac endoderm and was not discernible in the AX or hindgut invagination (Fig. 10G). At this time, afadin was strongest in the VCM (Fig. 10G), but strong diffuse staining also localized to the DCM and underlying core cells (Fig. 10H). By 7-s, VCM afadin persisted as the latter extended over the nascent omphalomesenteric artery (Fig. 10I). Finally, the ACD region never exhibited levels of afadin stronger than any other core cells.

In light of these collective results, we re-examined localization of alpha-4-integrin, previously remarked upon in the dorsal region of the allantois (Downs, 2002). At all stages (EB-6-s), alpha-4-integrin was detectable only in the single layer of mesothelial cells that constitute what we call here the DCM (Fig. 11A–C), further underscoring distinct differences between the VCM, DCM and distal mesothelial surface.

DISCUSSION

We report that, by comparison with yolk sac endoderm, mesothelium of the allantois does not appear to be a typical epithelium. Nevertheless, allantoic mesothelium exhibits regionally distinct morphological, functional and molecular properties both at the time of the appearance of the allantoic bud, and during the bud's elongation period, just prior to union with the chorion and tail rotation.

On the basis of our findings, we conclude that the mesothelial cells over much of the allantois have incomplete junctional complexes and are less consistently polarized than a more typical epithelium. Consequently, allantoic mesothelial cells would not be expected to modulate differences between the internal and external environments to as great an extent as an epithelium with consistent tight junctions. Regional variations in this overall arrangement may form the basis for differential mesothelial permeability observed with BDA challenge. Specifically, cell shape may influence the number of intercellular adhesion points and affect mesothelial permeability, with squamous distal mesothelium and its few contact points more porous than cuboidal proximal mesothelium and its more numerous ones. Nevertheless, VCM and DCM, while similar in cell shape, ultrastructure, and possibly numbers of contact points, exhibited distinct permeability differences, with VCM impermeable to high- and low-MW BDA, whereas DCM was impermeable only to higher MW BDA.

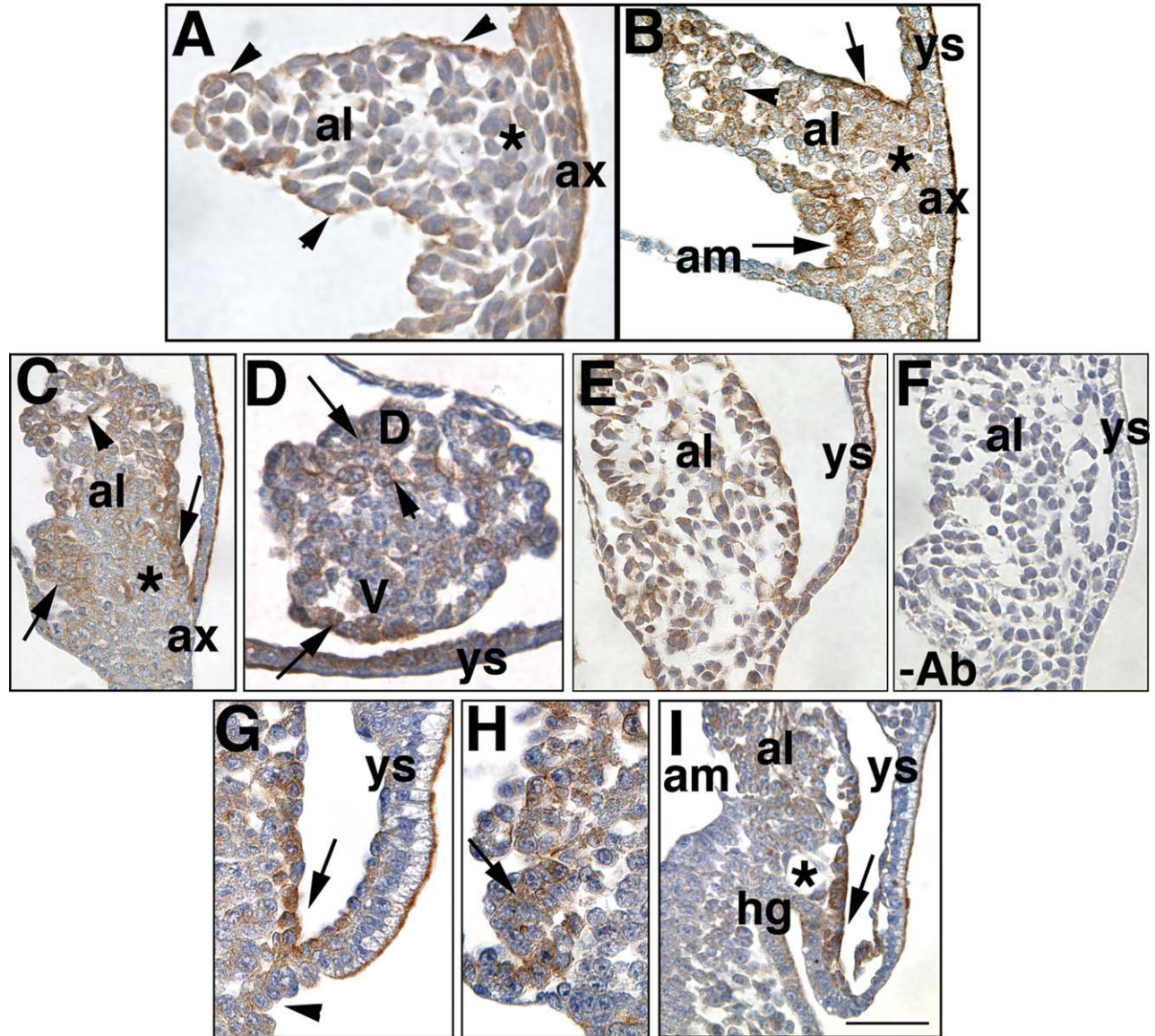


Fig. 10. Localization of afadin (AF-6) to the allantois and surrounding tissues. (A) LB stage. Arrowheads indicate intense afadin on allantoic mesothelium. Asterisk, ACD region; ax, allantois-associated extraembryonic visceral endoderm. (B) EHF stage. Upper arrow, VCM; lower arrow, DCM; arrowhead, example of afadin-positive inner core cell; asterisk, ACD. (C–F) 4-s stage. Sagittal (C) and transverse (D) sections show strong afadin in the VCM (upper arrowhead in (C), lower arrowhead in (D)), diffuse afadin in DCM and underlying core cells (lower arrow in (C), upper arrow in (D)), and positive inner core cells (arrowheads, C, D). Positive (E) and corresponding negative (F, minus antibody, -Ab) controls. (G, H) 6-s stage. VCM (G), arrow, afadin-negative hindgut invagination, arrowhead; DCM (H), arrow. (I) 7-s stage. Arrow indicates afadin-positive VCM that appears to be spreading over the developing omphalomesenteric artery that is elongating from its putative site of origin in the VOC (asterisk). Scale bar in (I) = 50 μ m (C, E, F, I); 75 μ m (D, G, H); 116 μ m (B); 90 μ m (A).

The basis for these differences is not clear. One possibility is that VCM cells contain more or qualitatively different contact points. This is supported by the relative differences in ZO-1 intensity in the VCM and DCM, with ZO-1 darker and more concentrated in the VCM (Fig. 5 and 9). Alternatively, VCM cells may be associated with an extracellular matrix that may plug gaps between its cells, similar to the intestinal epithelium as the latter undergoes renewal (Watson et al., 2009). For

example, although results of TEM here and in a previous study in the rat allantois (Ellington, 1985) did not reveal the presence of a basal lamina beneath the allantoic mesothelium at any stage, we had recently demonstrated that what we here recognize as the VCM was associated with robust perlecan and Col IV, both proteins of which are found in extracellular matrix (Mikedis and Downs, 2009). In particular, while Col IV cannot be part of an allantoic basal lamina, it appeared in a

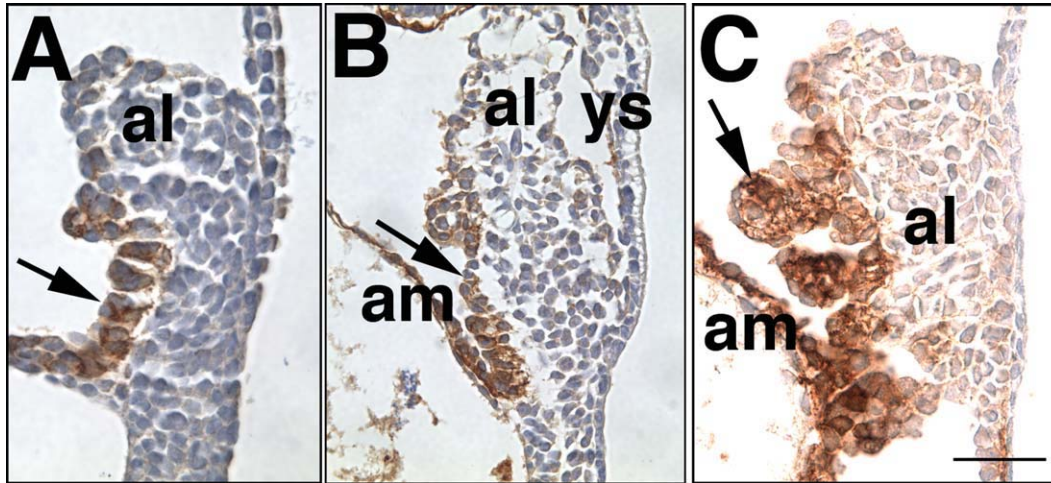


Fig. 11. Localization of alpha-4-integrin to the DCM. LM. In all panels, the arrow indicates the alpha-4-integrin-positive DCM. (A) LB stage. (B) 3-s stage. (C) 4-s stage, transverse orientation. Scale bar in (C) = 50 μ m (B); 75 μ m (A, C).

previous study (Mikedis and Downs, 2009) to circumscribe the ACD, part of it localizing beneath the VCM. There, it might prevent the passage of and/or sequester substances from the exocoelom into the underlying allantoic core.

Regionalization and Porosity of the Allantoic Mesothelium: A Role in Vascular Patterning?

The use of BDAs provided evidence that each mesothelial subtype, distal, DCM and VCM, may be intimately linked to its underlying core cells. We had previously shown through grafting that the allantois exhibited distal, mid- and proximal regionalization by headfold stages (Downs and Harmann, 1997; Downs, 1998). Specifically, when distal region cells were grafted into the base of the allantois, they returned to the distal allantois, while proximal cells remained within the proximal region of the allantois. Immunohistochemical analyses further supported compartmentalization of the allantois, revealing that distal mesothelium and its underlying cells expressed VCAM-1 (Downs, 2002) at a consistent distance from the embryonic junction by headfold stages (Downs et al., 2004), while alpha-4-integrin was associated with the DCM (see Downs, 2002, and this study).

Thus, the allantois may be compartmentalized into distinct regions by the headfold stage. On that basis, we propose that allantoic mesothelium is involved in establishing the vascular pattern of the nascent umbilical artery. We had previously observed that the primary umbilical artery is patterned over time (Inman and Downs, 2006b). It consists of a simple proximal "stem" that fans out distally into a highly branched network of vessels

(Naiche and Papaioannou, 2003; Inman and Downs, 2006b). This pattern is undoubtedly functionally significant. Distally, the branched network of allantoic vessels would become distributed along most of the chorionic plate as the allantois spreads onto it during early placental morphogenesis, penetrating it and creating a large surface area by which nutrients, wastes, and gases are exchanged with the mother (Cross et al., 2003; Fig. 2D). Proximally, and by contrast, the relatively simple unbranched stem connects to the VOC, which is ventrally positioned in the allantoic core and lies beneath the VCM (Downs et al., 1998; Inman and Downs, 2006b). Although poorly characterized, the VOC channels the entire arterial circulatory system of the conceptus into the umbilical cord. Distal and proximal regions of the allantoic mesothelium may, therefore, reflect unique functions in branching and channeling of the nascent umbilical vasculature.

Given these and the observation that the allantois is bathed over much of its surface in exocoelomic fluid, we propose a model by which porous distal mesothelium may permit the diffusion of factors from exocoelomic fluid that might act upon distal endothelial cells to promote vascular branching, while the impermeable VCM, which overlies the unbranched stem of the nascent arterial system, prevents such passage, and inhibits proximal branching (Fig. 12). Although the factors involved in umbilical patterning are not known, some candidate molecules may be members of the Fibroblast Growth Factor (FGF) family, many of which are angiogenic factors. Most FGFs have molecular weights between 17,000 and 34,000 (Ornitz and Itoh, 2001); as revealed in this study, distal mesothelium is permeable to BDA of molecular weight as high as 500,000, whereas proximal mesothelium

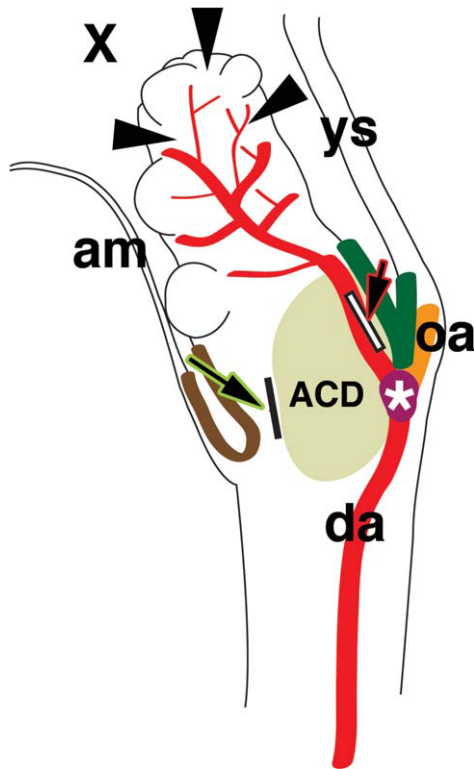


Fig. 12. Model for the role of mesothelial permeability in patterning the allantoic vasculature. Schematic diagram of a sagittal view of the allantois. Distal arrowheads indicate potential flow from the exocoelom into the permeable distal mesothelium of the allantois. The result is a branched arterial system that will spread over the chorion. Left large arrow stroked with green indicates communication from the amnion and/or exocoelom through the dorsal cuboidal mesothelium (DCM) (dark brown color) to its underlying layers, but stopping at the allantoic core domain (ACD), which is protected from flow (dark green color and large arrow stroked with red) by the Ventral Cuboidal Mesothelium (VCM) (blocked at white rectangle). The result of VCM protection is an unbranched arterial stem that fuses precisely at the Vessel of Confluence (VOC, white asterisk) with the pre-omphalomesenteric artery (oa) of the visceral yolk sac (ys), and the right and left paired dorsal aortic arteries of the fetus (da, shown in side view).

is not. Of course, other factors such as protein shape, charge, and post-translational modifications may be as important as molecular size in the ability to weave through mesothelial junctions. Nevertheless, molecules between 3,000 and 500,000 MW may be able to diffuse between cells of the distal mesothelium and promote vascular branching, whereas they cannot get through proximal mesothelium, where underlying endothelial cells form an unbranched vascular stem. FGFs require heparan sulfate proteoglycans (HSPG) as coreceptors for their interactions with specific FGF receptors (Javerzat et al., 2002). Although perlecan, an HSPG, and *Fgf8* have been identified in the allantois (Crossley and Martin, 1995; Mikedis and Downs, 2009), little is known about the spatio-

temporal whereabouts, if any, of most FGFs and their receptors there. Mouse embryos lacking *Fgfr2* protein exhibited reduced vascularization and failed to form a labyrinth (Xu et al., 1998), suggesting that FGFs are involved in branching vascularization of the allantois. However, whether *Fgfr2* localizes to the allantois and/or chorion is not known.

Unfortunately, the nature and content of the exocoelomic cavity are poorly characterized. The exocoelomic cavity is delimited by the chorion, visceral yolk sac, amnion, and mesothelial surface of the allantois. Only the yolk sac has been characterized for its role in contributing to the content of the exocoelom. Exocoelomic fluid contains immunoglobulins passively transferred by the yolk sac from the mother (Brambell, 1966), as well as proteins both actively transported and manufactured by this tissue (Huxham and Beck, 1984). These include alpha-fetoprotein, albumen, prealbumen, alpha-antitrypsin, transferrin, embryo-specific alpha globulin, and conalbumen. However, a number of other proteins remain uncharacterized. Therefore, which growth factors are present in the exocoelom, and from where they come, is obscure.

The exocoelom may not be the only source of factors that enter the porous allantoic mesothelium. Given that the allantois grows through this cavity in close association with the adjacent amnion and yolk sac (Fig. 1E), it is possible that these tissues are a source of vascular/hematopoietic inducing signals that are transmitted through direct contact. For example, the yolk sac endoderm promotes vasculogenesis and hematopoiesis of yolk sac mesoderm through hedgehog signaling (Dyer et al., 2001). Perhaps, endoderm-derived hedgehog signaling (Becker et al., 1997; Farrington et al., 1997) acts on the allantois to promote these processes there, as previous results have indicated that the allantois not only undergoes vasculogenesis (Downs et al., 1998) but also has hematopoietic potential, as well (Zeigler et al., 2006). However, whether hedgehog signaling is involved in allantoic vasculogenesis is not clear; for example, while abrogation of hedgehog signaling affects yolk sac vascularization, it seems not to have a direct effect on vascularization of the allantois (Astorga and Carlsson, 2007). However, patterning and hematopoiesis were not examined in this study.

Alternatively, allantoic mesothelium may play a role in the biology of its adjacent tissues, as the ultrastructure of the proximal walls suggested roles in protein production and secretion. For example, whilst the mammalian amnion is not generally vascularized, ectopic blood vessels have been observed there in *Smad5* mutants (Chang et al., 1999; Bosman et al., 2006), suggesting that the murine amnion has the potential to vascularize but is normally suppressed from doing so. Perhaps contact with the mouse allantois suppresses amniotic vascularization

in this species. Indeed, Smad5 localizes to the amnion (Chang et al., 1999), while BMP-4, which can inhibit downstream gene expression through Smad5 (Yamamoto et al., 1997; Nishimura et al., 1998), is found in allantoic mesothelium at all stages (Lawson et al., 1999; Downs et al., 2004).

Lability and Blebbing of the Allantoic Mesothelium: Roles in Placental Morphogenesis and/or Hematopoiesis?

While permeability of the allantoic surface may play a role in vascular patterning, why tight junctions are not involved in the selective permeability we observed is not clear. One possibility is that, distally, a labile mesothelium may be required for transformation of the distal tip of the allantois into a major component of the placental labyrinth. One of us had shown that chorio-allantoic fusion is mediated by the mesothelial surfaces of the allantois and chorion (Downs and Gardner, 1995). Although the fate of these mesothelial surfaces is still not known, it is tantalizing to speculate that the lack of junctional complexes on mesothelium may facilitate the latter's breakdown to allow the allantoic vasculature to penetrate the chorion or differentiation into appropriate allantoic cell types of the labyrinth.

Alternatively, lability of the mesothelium may promote mesothelial differentiation into components of the vascular and hematopoietic systems. Although previous authors commented that allantoic blebs bore a superficial resemblance to yolk sac blood islands, they concluded that this was as far as the similarities went, as they found no evidence for the presence of blood islands in the allantois (Tamarin and Boyde, 1976). Nevertheless, given the persistence of these blebs through the 8-s stage, it is possible that the blebs may function as microniches for the eventual formation of definitive hematopoietic cells. The latter were identified on the surface of the allantois after several days in explant culture (Zeigler et al., 2006), and within the chorio-allantoic placenta at 11.5 dpc (Gekas et al., 2005; Otterbach and Dzierzak, 2005). Indeed, we have observed the presence of extracellular matrix within allantoic blebs that might promote hematopoiesis there (Mikedis and Downs, 2009).

Another role for a permeable mesothelium, possibly concomitant with hematopoiesis, may be to aid the spread of the allantois onto the chorion, similar to the rolling mechanism used by hematopoietic cells along bone marrow sinusoidal endothelial cells to home to the bone marrow (Chute, 2006). Many molecular homing components are found in the allantois, such as integrins (Yang et al., 1993; Downs, 2002), VCAM-1 (Gurtner et al., 1995; Kwee et al., 1995; Downs, 2002), and PECAM-1 (Naiche and Papaioannou, 2003; Inman and Downs, 2006b).

At the same time, blebs covered by mesothelium could provide a reserve of mesothelial-committed cells that could cover the expanding allantois without the immediate need for recruitment of new mesothelial cells. Thus, the blebs could provide a ready source of cell membranes necessary for formation of the chorionic labyrinth. A role in the process of chorio-allantoic union for the blebs, described as "spheroidal cells," had previously been speculated upon (Tamarin and Boyde, 1976).

Potential Roles for E-Cadherin, ZO-1, and Afadin in the Allantois

Although abundant E-cadherin protein was observed in the murine visceral yolk sac at all stages, allantoic E-cadherin was detectable only within the presumptive ACD, despite an abundance of adhesion complexes in the allantoic mesothelium. Allantoic E-cadherin in the proximal core is consistent with a role in the origin of the primordial germ cells (Okamura et al., 2003), which are thought to originate within or near what we now know to be the ACD (Chiquoine, 1954; Ozdzinski, 1967). Thus, E-cadherin does not appear to play a role in the biology of nascent allantoic mesothelium and its adhesion complexes.

By contrast with E-cadherin, ZO-1 was abundant throughout the allantois at all stages, appearing as punctate and discontinuous spots within and between inner and outer cell populations. Although recent evidence suggests that ZO-1 and related proteins are critical regulators of tight junction assembly in some cell types (Fanning and Anderson, 2009; Tsukita et al., 2009), they are also components of the adhesion junction in nonepithelial cells, such as fibroblasts and cardiomyocytes; cells lacking ZO proteins have been shown to have defects in assembly of adherens junctions (reviewed in Fanning and Anderson, 2009). Our data suggest that ZO-1 may play a role in assembly of adhesion junctions in allantoic mesodermal cells, rather than in tight junction formation. A number of other proteins, such as occludin and claudin, are found in tight junctions and may be useful in future for determining if allantoic mesothelium ever forms a conventional epithelial surface (Steed et al., 2010).

Afadin acts as a scaffold protein that links nectin family cell adhesion proteins to actin-binding proteins and intracellular signaling pathways (Rikitake and Takai, 2008; Takai et al., 2008), thus possibly coordinating cell signaling with cytoskeletal rearrangements. Afadin was strongly expressed in the VCM, suggesting that it may play a role in cell signaling there. For example, recent evidence suggests that afadin attenuates vascular endothelial growth factor (VEGF; Tawa et al., 2010), whose presence was noted in what we here recognize as the VCM (Miquerol et al., 1999).

Given that the VCM overlies the unbranched portion of the nascent umbilical artery, which contains Flk-1 (Downs et al., 1998), one of VEGFs major receptors (Yamaguchi et al., 1993), afadin may modulate VEGF and thus, vascularization of the proximal stem. Afadin is also involved in attenuation of Platelet Derived Growth Factor (PDGF; Nakata et al., 2007), which has been found in allantoic mesoderm and is required for labyrinth formation (Ohlsson et al., 1999). Thus, afadin's role in signaling and establishment of new adhesion points allows us to presume that robust afadin localization to the VCM may be essential for coordinating the signaling and cytoskeletal changes necessary for the multitude of processes that occur in the understudied posterior embryonic region.

CONCLUSIONS

The rodent allantois is thought to be unique amongst placental mammalian umbilical cords in not having an endodermal component (Mossman, 1987). Results of this study further support that conclusion, as we found no evidence for an endodermal component of the allantoic surface. However, the proximal walls of the allantois, like endoderm, were cuboidal in shape and exhibited an ultrastructure more conducive to protein synthesis than those of the distal mesothelium. In that regard, the proximal allantoic walls may act less like a transporting epithelium and more like a synthetic one, and thus, produce factors that influence decisions in associated tissues. For example, given its position over the ACD, the VCM may play a role in regulating the proliferative and differentiative properties of this core region, which is essential for elongation to the chorion. By contrast, the DCM, which exhibited similar ultrastructure but greater porosity and differential gene expression, might play a distinctly different role in the biology of the allantois. Unfortunately, very few systematic studies have been carried out on this major embryonic appendage. We anticipate that results of this study will provide a sound foundation upon which to build a systematic and coherent understanding of the role of the allantois as the interface between the mother and fetus.

ACKNOWLEDGMENTS

The authors are grateful to Dr. Shannon Gifford for help with histological morphology; Jacqueline McHugh and Professor Ralph Albrecht for assistance with SEM; Robin Lindeman for suggesting afadin and for technical assistance with BDA staining and immunohistochemistry for afadin and ZO-1; Joanne Beyer for help with ZO-1 control staining; Amanda Roehl for assistance with animal husbandry and calculation of the exocoelomic fluid

volume; and Randall Massey and Ben August (Electron Microscopy Facility, UW-Madison School of Medicine and Public Health), and Dr. Kimberly Inman for help with TEM.

LITERATURE CITED

- Astorga J, Carlsson P. 2007. Hedgehog induction of murine vasculogenesis is mediated by Foxf1 and Bmp4. *Development* 134:3753–3761.
- Beck F, Lloyd JB, Griffiths A. 1967. A histochemical and biochemical study of some aspects of placental function in the rat using maternal injection of horseradish peroxidase. *J Anat* 101:461–478.
- Becker S, Wang ZJ, Massey H, Arauz A, Labosky P, Hammerschmidt M, St.-Jacques B, Bumcrot D, McMahon AP, Grabel L. 1997. A role for Indian hedgehog in extraembryonic endoderm differentiation in F9 cells and the early mouse embryo. *Dev Biol* 187:298–310.
- Bosman EA, Lawson KA, Debruyn J, Beek L, Francis A, Schoonjans L, Huylebroeck D, Zwijsen A. 2006. Smad5 determines murine amnion fate through the control of bone morphogenetic protein expression and signaling levels. *Development* 133:3399–3409.
- Brambell FWR. 1966. The transmission of immunity from mother to young and catabolism of immunoglobins. *Lancet* ii:1087–1093.
- Champlin AK, Dorr DL, Gates AH. 1973. Determining the stage of the estrous cycle in the mouse by the appearance of the vagina. *Biol Reprod* 8:491–494.
- Chang H, Huylebroeck D, Verschueren K, Guo Q, Matzuk MM, Zwijsen A. 1999. Smad5 knockout mice die at mid-gestation due to multiple embryonic and extraembryonic defects. *Development* 126:1631–1642.
- Chiquoine AD. 1954. The identification, origin, and migration of the primordial germ cells in the mouse embryo. *Anat Rec* 118:135–146.
- Chute J. 2006. Stem cell homing. *Curr Opin Hematol* 13:399–406.
- Cross JC, Simmons GJ, Watson ED. 2003. Chorion-allantoic morphogenesis and formation of the placental villous tree. *Ann N Y Acad Sci* 995:84–93.
- Crossley PH, Martin GM. 1995. The mouse Fgf8 gene encodes a family of polypeptides and is expressed in regions that direct outgrowth and patterning in the developing embryo. *Development* 121:439–451.
- Downs KM. 1998. The murine allantois. *Curr Top Dev Biol* 39:1–33.
- Downs KM. 2002. Early placentation in the mouse. *Placenta* 23:116–131.
- Downs KM. 2006. In vitro methods for studying vascularization of the murine allantois and allantoic union with the chorion. *Methods Mol Med* 121:241–272.
- Downs KM. 2008. Systematic localization of Oct-3/4 to the gastrulating mouse conceptus suggests manifold roles in mammalian development. *Dev Dyn* 237:464–475.
- Downs KM. 2009. Enigmatic primitive streak: Prevailing notions and challenges concerning the body axis of mammals. *Bioessays* 31:892–902.
- Downs KM, Davies T. 1993. Staging of gastrulation in mouse embryos by morphological landmarks in the dissection microscope. *Development* 118:1255–1266.
- Downs KM, Gardner RL. 1995. An investigation into early placental ontogeny: Allantoic attachment to the chorion is selective and developmentally regulated. *Development* 121:407–416.
- Downs KM, Harmann C. 1997. Developmental potency of the murine allantois. *Development* 124:2769–2780.
- Downs KM, Gifford S, Blahnik M, Gardner RL. 1998. The murine allantois undergoes vasculogenesis that is not accompanied by erythropoiesis. *Development* 125:4507–4521.

- Downs KM, McHugh J, Copp AJ, Shtivelman E. 2002. Multiple developmental roles of Ahnak are suggested by localization to sites of placentation and neural plate fusion in the mouse conceptus. *Mech Dev* 119S:S31–S38.
- Downs KM, Hellman ER, McHugh J, Barrickman K, Inman K. 2004. Investigation into a role for the primitive streak in development of the murine allantois. *Development* 131:37–55.
- Downs KM, Inman KE, Jin DX, Enders AC. 2009. The Allantoic Core Domain (ACD): New insights into development of the murine allantois and its relation to the primitive streak. *Dev Dyn* 238:532–553.
- Dyer MA, Farrington SM, Mohn D, Munday JR, Baron MH. 2001. Indian hedgehog activates hematopoiesis and vasculogenesis and can respect prospective neuroectodermal cell fate in the mouse embryo. *Development* 128:1717–1730.
- Ellington SKL. 1985. A morphological study of the development of the allantois of rat embryos in vivo. *J Anat* 142:1–11.
- Enders AC, Blankenship TN, Conley AJ, Jones CJP. 2006. Structure of the midterm placenta of the spotted hyena, *Crocuta crocuta*, with emphasis on the diverse hemophagous regions. *Cells Tissues Organs* 183:141–155.
- Fanning AS, Anderson JM. 2009. Zonula Occludens-1 and -2 are cytosolic scaffolds that regulate the assembly of cellular junctions. *Ann N Y Acad Sci* 1165:113–120.
- Farquhar MG, Palade GE. 1963. Junctional complexes in various epithelia. *J Cell Biol* 17:375–412.
- Farrington SM, Belaoussoff M, Baron MH. 1997. Winged-helix, Hedgehog and Bmp genes are differentially expressed in distinct cell layers of the murine yolk sac. *Mech Dev* 62:197–211.
- Gekas C, Dieterlen-Lievre F, Orkin SH, Mikkola HKA. 2005. The placenta is a niche for hematopoietic stem cells. *Dev Cell* 8:365–375.
- Gurtner GC, Davis V, Li H, McCoy MJ, Sharpe A, Cybulsky MI. 1995. Targeted disruption of the murine VCAM1 gene: Essential role of VCAM-1 in chorioallantoic fusion and placentation. *Genes Dev* 9:1–14.
- Haar JL, Ackerman GA. 1971. A phase and electron microscopic study of vasculogenesis and erythropoiesis in the yolk sac of the mouse. *Anat Rec* 170:199–223.
- Harstock A, Nelson WJ. 2008. Adherens and tight junctions: Structure, function and connections to the actin cytoskeleton. *Biochem Biophys Acta* 1778:660–669.
- Huxham IM, Beck F. 1984. Characterization of exocoelomic fluid protein from rat conceptuses cultured in rat and human sera: A measure of yolk sac activity during organogenesis. *J Embryol Exp Morph* 84:203–215.
- Ikeda W, Nakanishi H, Miyoshi J, Madai K, Ishizaki H, Tanaka M, Togawa A, Takahashi K, Nishioka H, Yoshida H, Mizoguchi A, Nishikawa S, Takai Y. 1999. Afadin: A key molecule essential for structural organization of cell-cell junctions of polarized epithelia during embryogenesis. *J Cell Biol* 146:1117–1131.
- Inman K, Downs KM. 2006a. Localization of Brachyury (T) in embryonic and extraembryonic tissues during mouse gastrulation. *Gene Exp Patterns* 6:783–793.
- Inman KE, Downs KM. 2006b. Brachyury is required for elongation and vasculogenesis in the murine allantois. *Development* 133:2947–2959.
- Javerzat S, Auguste P, Bikfalvi A. 2002. The role of fibroblast growth factors in vascular development. *Trends Mol Med* 8:483–489.
- King BF, Enders AC. 1970. Protein absorption and transport by the guinea pig visceral yolk sac placenta. *Am J Anat* 129:261–288.
- Kingsley PD, McGrath KE, Maltby KM, Koniski AD, Ramchandran R, Palis J. 2001. Subtractive hybridization reveals tissue-specific expression of ahnak during embryonic development. *Develop Growth Differ* 43:133–143.
- Kwee L, Baldwin HS, Shen HM, Steward CL, Buck C, Buck CA, Labow MA. 1995. Defective development of the embryonic and extraembryonic circulatory systems in vascular cell adhesion molecule (VCAM-1) deficient mice. *Development* 121:489–503.
- Lawson KA, Dunn NR, Roelen BA, Zeinstra LM, Davis AM, Wright CV, Korving JP, Hogan BL. 1999. Bmp4 is required for the generation of primordial germ cells in the mouse embryo. *Genes Dev* 13:424–436.
- Mandai K, Nakanishi H, Satoh A, Obashi H, Wada M, Nishioka H, Itoh M, Mizoguchi A, Aoiki T, Fujimoto T, Matsuda Y, Tsukita S, Takai Y. 1997. Afadin: A novel actin filament-binding protein with one PDZ domain localized at cadherin-based cell-to-cell adherens junctions. *J Cell Biol* 139:517–528.
- Mikedis MM, Downs KM. 2009. Collagen type IV and perlecan exhibit concentrated and dynamic localization in the Allantoic Core Domain, a putative stem cell niche in the murine allantois. *Dev Dyn* 238:3193–3204.
- Miquerol L, Gertsenstein M, Harpal K, Rossant J, Nagy A. 1999. Multiple developmental roles of VEGF suggested by a LacZ-tagged allele. *Dev Biol* 212:307–322.
- Mossman HW. 1987. Vertebrate fetal membranes. New Brunswick: Rutgers University Press.
- Naiche LA, Papaioannou VE. 2003. Loss of *Tbx4* blocks hindlimb development and affects vascularization and fusion of the allantois. *Development* 130:2681–2693.
- Nakata S, Fujita N, Kitagawa Y, Okamoto R, Ogita H, Takai Y. 2007. Regulation of platelet-derived growth factor receptor activation by afadin through SHP-2: Implications for cellular morphology. *J Biol Chem* 282:37815–37825.
- Nishimura R, Kato Y, Chen D, Harris SE, Mundy GR, Yoneda T. 1998. Smad5 and DPC4 are key molecules in mediating BMP-2-induced osteoblastic differentiation of the pluripotent mesenchymal precursor cell line C2C12. *J Biol Chem* 273:1872–1879.
- Ohlsson R, Falck P, Hellstrom M, Lindahl P, Bostrom H, Franklin G, Ahrlund-Richter L, Pollard J, Soriano P, Betsholtz C. 1999. PDGFB regulates the development of the labyrinthine layer of the mouse fetal placenta. *Dev Biol* 212:124–136.
- Okamura D, Kimura T, Nakano T, Matsui Y. 2003. Cadherin-mediated cell interaction regulates germ cell determination in mice. *Development* 130:6423–6430.
- Ornitz DM, Itoh N. 2001. Fibroblast growth factors. *Genome Biol* 2: reviews3005-reviews3005.12.
- Otterbach K, Dzierzak E. 2005. The murine placenta contains hematopoietic stem cells within the vascular labyrinth region. *Dev Cell* 8:377–387.
- Ozdzenski W. 1967. Observations on the origin of primordial germ cells in the mouse. *Zool Pol* 17:367–381.
- Paria BC, Zhao X, Das SK, Dey SK, Yoshinaga K. 1999. Zonula occludens-1 and E-cadherin are coordinately expressed in the mouse uterus with the initiation of implantation and decidualization. *Dev Biol* 208:488–501.
- Reiner A, Veenman CL, Medina L, Jiao Y, Del Mar N, Honig MG. 2000. Pathway tracing using biotinylated dextran amines. *J Neurosci Methods* 103:23–37.
- Rikitake Y, Takai Y. 2008. Interactions of the cell adhesion molecule nectin with transmembrane and peripheral membrane proteins for pleiotropic functions. *Cell Mol Life Sci* 65:253–263.
- Snell GB, Stevens LC. 1966. Early embryology. In: Green EL, editor. *Biology of the Laboratory Mouse*. New York: McGraw Hill. pp205–245.
- Steed E, Balda MS, Matter K. 2010. Dynamics and functions of tight junctions. *Trends Cell Biol* 20:142–149.
- Takai Y, Nakanishi H. 2003. Nectin and afadin: novel organizers of intercellular junctions. *J Cell Sci* 116:17–27.
- Takai Y, Ikeda W, Ogita H, Rikitake Y. 2008. The immunoglobulin-like cell adhesion molecule nectin and its associated protein afadin. *Ann Rev Cell Dev Biol* 24:309–342.
- Tamarin A, Boyde A. 1976. Three-dimensional anatomy of the 8-day mouse conceptus: A study by scanning electron microscopy. *J Embryol Exp Morphol* 36:575–596.
- Tawa H, Rikitake Y, Takahashi M, Amano H, Miyata M, Satomi-Kobayashi S, Kinugasa M, Nagamatsu Y, Majima T, Ogita H, Miyoshi J, Hirata K, Takai Y. 2010. Role of afadin in vascular endothelial growth factor- and sphingosine 1-phosphate-induced angiogenesis. *Circ Res* 106:1731–1742.

- Tsukita S, Katsuno T, Yamazaki T, Umeda K, Tamura A, Tsukita S. 2009. Roles of ZO-1 and ZO-2 in establishment of the belt-like adherens and tight junctions with paracellular permselective barrier function. *Ann NY Acad Sci* 1165:44–52.
- Uy GD, Downs KM, Gardner RL. 2002. Inhibition of trophoblast stem cell potential in chorionic ectoderm coincides with occlusion of the ectoplacental cavity in the mouse. *Development* 129:3913–3924.
- Veenman CL, Reiner A, Honig MG. 1992. Biotinylated dextran amine as an anterograde tracer for single- and double-labeling studies. *J Neurosci Methods* 41:239–254.
- Watson AJM, Juckworth CA, Guan Y, Montrose MH. 2009. Mechanisms of epithelial cell shedding in the mammalian intestine and maintenance of barrier function. *Ann N Y Acad Sci* 1165:135–162.
- Xu X, Weinstein M, Li C, Naski M, Cohen RI, Ornitz DM, Leder P, Deng C. 1998. Fibroblast growth factor receptor 2 (FGFR2)-mediated reciprocal regulation loop between FGF8 and FGF10 is essential for limb induction. *Development* 125:753–765.
- Yamaguchi TP, Dumont DJ, Conlon RA, Breitman ML, Rossant J. 1993. flk-1, an flt-related receptor tyrosine kinase, is an early marker for endothelial cell precursors. *Development* 118:488–498.
- Yamamoto N, Akiyama S, Katagiri T, Namiki M, Kurokawa T, Suda T. 1997. Smad1 and Smad5 act downstream of intracellular signaling of BMP-2 that inhibits myogenic differentiation and induces osteoblast differentiation in C2C12 myoblasts. *Biochem Biophys Acta* 238:574–580.
- Yang JT, Rayburn H, Hynes RO. 1993. Embryonic mesodermal defects in $\alpha 4$ integrin-deficient mice. *Development* 119:1093–1105.
- Yokoyama S, Tachibana K, Nakanishi H, Yamamoto Y, Irie K, Madndai K, Nagafuchi A, Monden M, Takai Y. 2001. Alpha-catenin-independent recruitment of ZO-1 to nectin-based cell-cell adhesion sites through afadin. *Mol Biol Cell* 12:1595–1605.
- Zeigler BM, Sugiyama D, Chen M, Guo Y, Downs KM, Speck NA. 2006. The allantois and chorion, which are isolated before circulation or chorio-allantoic fusion, have hematopoietic potential. *Development* 133:4183–4192.